

Micromagnetism

Lukas Exl, Dieter Suess and Thomas Schrefl

Abstract Computational micromagnetics is widely used for the design and development of magnetic devices. The theoretical background of these simulations is the continuum theory of micromagnetism. It treats magnetization processes on a significant length scale which is small enough to resolve magnetic domain walls and large enough to replace atomic spins by a continuous function of position. The continuous expression for the micromagnetic energy terms are either derived from their atomistic counterpart or result from symmetry arguments. The equilibrium conditions for the magnetization and the equation of motion are introduced. The focus of the discussion lies on the basic building blocks of micromagnetic solvers. Numerical examples illustrate the micromagnetic concepts. An open source simulation environment was used to address the ground state thin film magnetic element, initial magnetization curves, stress-driven switching of magnetic storage elements, the grain size dependence of coercivity of permanent magnets, and damped oscillations in magnetization dynamics.

Lukas Exl

Lukas Exl, Faculty of Mathematics, University of Vienna, Oskar-Morgenstern-Platz 1, 1090, Vienna, Austria e-mail: lukas.exl@univie.ac.at

Dieter Suess

Dieter Suess, Christian Doppler Laboratory of Advanced Magnetic Sensing and Materials, Institute for Solid State Physics, TU Wien, Wiedner Hauptstrasse 8-10, 1040 Vienna, Austria e-mail: dieter.suess@tuwien.ac.at

Thomas Schrefl

Thomas Schrefl, Center for Integrated Sensor Systems, Danube University Krems, Viktor Kaplan Str. 2 E 2700 Wiener Neustadt e-mail: thomas.schrefl@donau-uni.ac.at

1 Introduction

Computer simulations are an essential tool for product design in modern society. This is also true for magnetic materials and their applications. The design of magnetic data storage systems such as hard discs devices [1, 2, 3, 4, 5] and random access memories [6, 7] relies heavily on computer simulations. Similarly, the computer models assist the development of magnetic sensors [8, 9] as used as biosensors or position and speed sensors in automotive applications [10]. Computer simulations give guidance for the advance of high performance permanent magnet materials [11, 12, 13] and devices. In storage and sensor applications the selection of magnetic materials, the geometry of the magnetically active layers, and the layout of current lines are key design question that can be answered by computations. In addition to the intrinsic magnetic properties, the microstructure including grain size, grain shape, and grain boundary phases is decisive for the magnet's performance. Computer simulations can quantify the influence of microstructural features on the remanence and the coercive field of permanent magnets.

The characteristic length scale of the above mentioned computer models is in the range of nanometers to micrometers. The length scale is too big for a description by spin polarized density functional theory. Efficient simulations by atomistic spin dynamics [14] are possible for nano-scale devices only. On the other hand, macroscopic simulations using Maxwell's equations hide the magnetization processes that are relevant for the specific functions of the material or device under consideration. Micromagnetism is a continuum theory that describes magnetization processes on significant length scales that is

- large enough to replace discrete atomic spins by a continuous function of position (the magnetization), but
- small enough to resolve the transition of the magnetization between magnetic domains

For most ferromagnetic materials this length scale is in the range of a few nanometers to micrometers for most ferromagnetic materials. The first aspect leads to a mathematical formulation which makes it possible to simulate materials and devices in reasonable time. Instead of billions of atomic spins, only millions of finite element have to be taken into account. The second aspect keeps all relevant physics so that the influence of structure and geometry on the formation of reversed domains and the motion of domain walls can be computed.

The theory of micromagnetism was developed well before the advance of modern computing technology. Key properties of magnetic materials can be understood by analytic or semi-analytic solutions of the underlying equations. However, the future use of powerful computers for the calculation of magnetic properties by solving the micromagnetic equations numerically was already proposed by Brown [15] in the late 1950s. The purpose of micromagnetics is

the calculation of the magnetization distribution as function of the applied field or the applied current taking into account the structure of the material and the mutual interactions between the different magnetic parts of a device.

2 Micromagnetic basics

The key assumption of micromagnetism is that the spin direction changes only by a small angle from one lattice point to the next [16]. The direction angles of the spins can be approximated by a continuous function of position. Then the state of a ferromagnet can be described by the continuous vector field, the magnetization $\mathbf{M}(\mathbf{x})$. The magnetization is the magnetic moment per unit volume. The direction of $\mathbf{M}(\mathbf{x})$ varies continuously with the coordinates x , y , and z . Here we introduced the position vector $\mathbf{x} = (x, y, z)^T$. Starting from the Heisenberg model [17, 18] which describes a ferromagnet by interacting spins associated with each atom, the micromagnetic equations can be derived whereby several assumptions are made:

1. Micromagnetism is a quasi-classical theory. The spin operators of the Heisenberg model are replaced by classical vectors.
2. The length of the magnetization vector is a constant that is uniform over the ferromagnetic body and only depends on temperature.
3. The temperature is constant in time and in space.
4. The Gibbs free energy of the ferromagnetic is expressed in terms of the direction cosines of the magnetization.
5. The energy terms are derived either by the transition from an atomistic model to a continuum model or phenomenologically.

In classical micromagnetism the magnetization can only rotate. A change of the length of \mathbf{M} is forbidden. Thus, a ferromagnet is in thermodynamic equilibrium, when the torque on the magnetic moment $\mathbf{M}dV$ in any volume element dV is zero. The torque on the magnetic moment $\mathbf{M}dV$ caused by a magnetic field \mathbf{H} is

$$\mathbf{T} = \mu_0 \mathbf{M}dV \times \mathbf{H}, \quad (1)$$

where μ_0 is the permeability of vacuum ($\mu_0 = 4\pi \times 10^{-7}$ Tm/A). The equilibrium condition (1) follows from the direct variation of the Gibbs free energy. If only the Zeeman energy of the magnet in an external field is considered, \mathbf{H} is the external field, \mathbf{H}_{ext} . In general additional energy terms will be relevant. Then \mathbf{H} has to be replaced by the effective field, \mathbf{H}_{eff} . Each energy term contributes to the effective field.

In the Sect. 3 we will derive continuum expressions for the various contributions to the Gibbs free energy functional using the direction cosines of the magnetization as unknown functions. In Sect. 5 we show how the equilib-

rium condition can be obtained by direct variation of the Gibbs free energy functional.

3 Magnetic Gibbs free energy

We describe the state of the magnet in terms of the magnetization $\mathbf{M}(\mathbf{x})$. In the following we will show how the continuous vector field $\mathbf{M}(\mathbf{x})$ is related to the magnetic moments located at the atom positions of the magnet.

3.1 Spin, magnetic moment, and magnetization

The local magnetic moment of an atom or ion at position \mathbf{x}_i is associated with the spin angular momentum, $\hbar\mathbf{S}$,

$$\boldsymbol{\mu}(\mathbf{x}_i) = -g\frac{|e|\hbar}{2m}\mathbf{S}(\mathbf{x}_i) = -g\mu_B\mathbf{S}(\mathbf{x}_i). \quad (2)$$

Here e is the charge of the electron, m is the electron mass, and g is the Landé factor. The Landé factor is $g \approx 2$ for metal systems with quenched orbital moment. The constant $\mu_B = 9.274 \times 10^{-24} \text{ Am}^2 = 9.274 \times 10^{-24} \text{ J/T}$ is the Bohr magneton. The constant \hbar is the reduced Planck constant, $\hbar = h/(2\pi)$, where h is the Planck constant. The magnetization of a magnetic material with N atoms per unit volume is

$$\mathbf{M} = N\boldsymbol{\mu}. \quad (3)$$

The magnetic moment is often given in Bohr magnetons per atom or Bohr magnetons per formula unit. The the magnetization is

$$\mathbf{M} = N_{\text{fu}}\boldsymbol{\mu}_{\text{fu}}, \quad (4)$$

where $\boldsymbol{\mu}_{\text{fu}}$ is the magnetic moment per formula unit and N_{fu} is the number of formula units per unit volume.

The length of the magnetization vector is assumed to be a function of temperature only and does not depend on the strength of the magnetic field:

$$|\mathbf{M}| = M_s(T) = M_s \quad (5)$$

where M_s is the saturation magnetization. In classical micromagnetism the temperature, T , is assumed to be constant over the ferromagnetic body and independent of time t . Therefore M_s is fixed and time evolution of the magnetization vector can be expressed in terms of the unit vector $\mathbf{m} = \mathbf{M}/|\mathbf{M}|$

$$\mathbf{M}(\mathbf{x}, t) = \mathbf{m}(\mathbf{x}, t)M_s. \quad (6)$$

The saturation magnetization of a material is frequently given as $\text{t}\mu_0 M_s$ in units of Tesla.

Example: The saturation magnetization is an input parameter for micro-magnetic simulations. In a multiscale simulation approach of the hysteresis properties of a magnetic materials it may be derived from the ab initio calculation of magnetic moment per formula unit. In NdFe₁₁TiN the calculated magnetic moment per formula unit is 26.84 $\text{t}\mu_B$ per formula unit [19]. The computed lattice constants were $a = 8.537 \times 10^{-10}$ m, $b = 8.618 \times 10^{-10}$ m, and $c = 4.880 \times 10^{-10}$ m [19] which give a volume of the unit cell of $v = 359.0 \times 10^{-30}$ m³. There are two formula units per unit cell and $N_{\text{fu}} = 2/v = 5.571 \times 10^{27}$. With (4) and (5) the saturation magnetization of NdFe₁₁TiN is $M_s = 1.387 \times 10^6$ A/m ($\mu_0 M_s = 1.743$ T).

3.2 Exchange energy

The exchange energy is of quantum mechanical nature. The energy of two ferromagnetic electrons depends on the relative orientation of their spins. When the two spins are parallel, the energy is lower than the energy of the antiparallel state. Qualitatively this behavior can be explained by the Pauli exclusion principle and the electrostatic Coulomb interaction. Owing to the Pauli exclusion principle two electrons can only be at the same place if they have opposite spins. If the spins are parallel the electrons tend to move apart which lowers the electrostatic energy. The corresponding gain in energy can be large enough so that the parallel state is preferred.

The exchange energy, E_{ij} , between two localized spins is [18]

$$E_{ij} = -2J_{ij}\mathbf{S}_i \cdot \mathbf{S}_j, \quad (7)$$

where J_{ij} is the exchange integral between atoms i and j , and $\hbar\mathbf{J}_i$ is the angular momentum of the spin at atom i . For cubic metals and hexagonal closed packed metals with ideal c over a ratio there holds $J_{ij} = J$. Treating the exchange energy for a large number of coupled spins, we regard E_{ij} as a classical potential energy and replace \mathbf{S}_i by a classical vector. Let \mathbf{m}_i be the unit vector in direction $-\mathbf{S}_i$. Then \mathbf{m}_i is the unit vector of the magnetic moment at atom i . If φ_{ij} is the angle between the vectors \mathbf{m}_i and \mathbf{m}_j the exchange energy is

$$E_{ij} = -2JS^2 \cos(\varphi_{ij}), \quad (8)$$

where $S = |\mathbf{S}_i| = |\mathbf{S}_j|$ is the spin quantum number.

Now, we introduce a continuous unit vector $\mathbf{m}(\mathbf{x})$, and assume that the angle φ_{ij} between the vectors \mathbf{m}_i and \mathbf{m}_j is small. We set $\mathbf{m}(\mathbf{x}_i) = \mathbf{m}_i$ and expand \mathbf{m} around \mathbf{x}_i

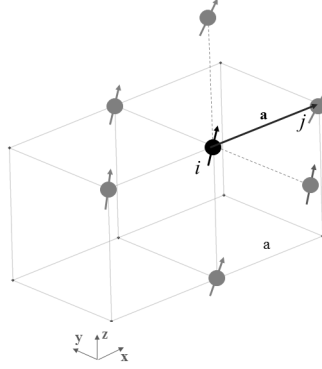


Fig. 1 Nearest neighbors of spin i for the calculation of the exchange energy in a simple cubic lattice.

$$\begin{aligned}
 \mathbf{m}(\mathbf{x}_i + \mathbf{a}_j) &= \mathbf{m}(\mathbf{x}_i) + \\
 &\frac{\partial \mathbf{m}}{\partial x} a_j + \frac{\partial \mathbf{m}}{\partial y} b_j + \frac{\partial \mathbf{m}}{\partial z} c_j + \\
 &\frac{1}{2} \left(\frac{\partial^2 \mathbf{m}}{\partial x^2} a_j^2 + \frac{\partial^2 \mathbf{m}}{\partial y^2} b_j^2 + \frac{\partial^2 \mathbf{m}}{\partial z^2} c_j^2 \right) + \dots
 \end{aligned} \tag{9}$$

Here $\mathbf{a}_j = (a_j, b_j, c_j)^\top$ is the vector connecting points \mathbf{x}_i and $\mathbf{x}_j = \mathbf{x}_i + \mathbf{a}_j$. We can replace $\cos(\varphi_{ij})$ by $\cos(\varphi_{ij}) = \mathbf{m}(\mathbf{x}_i) \cdot \mathbf{m}(\mathbf{x}_j)$ in (8). Summing up over the six nearest neighbors of a spin in a simple cubic lattice gives (see Fig. 1) the exchange energy of the unit cell. The vectors \mathbf{a}_j take the values $(\pm a, 0, 0)^\top$, $(0, \pm a, 0)^\top$, $(0, 0, \pm a)^\top$. For every vector \mathbf{a} there is the corresponding vector $-\mathbf{a}$. Thus the linear terms in the variable a in (9) vanish in the summation. The constant term, $\mathbf{m} \cdot \mathbf{m} = 1$, plays no role for the variation of the energy and will be neglected. The exchange energy of a unit cell in a simple cubic lattice is

$$\begin{aligned}
 \sum_{j=1}^6 E_{ij} &= -JS^2 \sum_{j=1}^6 \left(\mathbf{m}_i \cdot \frac{\partial^2 \mathbf{m}_i}{\partial x^2} a_j^2 + \mathbf{m}_i \cdot \frac{\partial^2 \mathbf{m}_i}{\partial y^2} b_j^2 + \mathbf{m}_i \cdot \frac{\partial^2 \mathbf{m}_i}{\partial z^2} c_j^2 \right) \\
 &= -2JS^2 a^2 \left(\mathbf{m}_i \cdot \frac{\partial^2 \mathbf{m}_i}{\partial x^2} + \mathbf{m}_i \cdot \frac{\partial^2 \mathbf{m}_i}{\partial y^2} + \mathbf{m}_i \cdot \frac{\partial^2 \mathbf{m}_i}{\partial z^2} \right)
 \end{aligned} \tag{10}$$

To get the exchange energy of the crystal we sum over all atoms i and divide by 2 to avoid counting each pair of atoms twice. We also use the relations

$$\mathbf{m} \cdot \frac{\partial^2 \mathbf{m}}{\partial x^2} = - \left(\frac{\partial \mathbf{m}}{\partial x} \right)^2, \tag{11}$$

which follows from differentiating $\mathbf{m} \cdot \mathbf{m} = 1$ twice with respect to x .

$$E_{\text{ex}} = \frac{JS^2}{a} \sum_i a^3 \left[\left(\frac{\partial \mathbf{m}_i}{\partial x} \right)^2 + \left(\frac{\partial \mathbf{m}_i}{\partial y} \right)^2 + \left(\frac{\partial \mathbf{m}_i}{\partial z} \right)^2 \right] \quad (12)$$

The sum in (12) is over the unit cells of the crystal with volume V . In the continuum limit we replace the sum with an integral. The exchange energy is

$$E_{\text{ex}} = \int_V A \left[\left(\frac{\partial \mathbf{m}_i}{\partial x} \right)^2 + \left(\frac{\partial \mathbf{m}_i}{\partial y} \right)^2 + \left(\frac{\partial \mathbf{m}_i}{\partial z} \right)^2 \right] dV. \quad (13)$$

Expanding and rearranging the terms in the bracket and introducing the nabla operator, ∇ , we obtain

$$E_{\text{ex}} = \int_V A \left[(\nabla m_x)^2 + (\nabla m_y)^2 + (\nabla m_z)^2 \right] dV. \quad (14)$$

In equations (13) and (14) we introduced the exchange constant

$$A = \frac{JS^2}{a} n. \quad (15)$$

In cubic lattices n is the number of atoms per unit cell ($n = 1, 2,$ and 4 for simple cube, body centered cubic, and face centered cubic lattices, respectively). In a hexagonal closed packed structures n is the ideal nearest neighbor distance ($n = 2\sqrt{2}$). The number N of atoms per unit volume is n/a^3 . At non-zero temperature the exchange constant may be expressed in terms of the saturation magnetization, $M_s(T)$. Formally we replace S by its thermal average. Using equations (2) and (3), we rewrite

$$A(T) = \frac{J [M_s(T)]^2}{(Ng\mu_B)^2 a} n. \quad (16)$$

The calculation of the exchange constant by (15) requires a value for the exchange integral, J . Experimentally, one can measure a quantity that strongly depends on J such as the Curie temperature, T_C , the temperature dependence of the saturation magnetization, $M_s(T)$, or the spin wave stiffness parameter, in order to determine J . According to the molecular field theory [20] the exchange integral is related to the Curie temperature given by

$$J = \frac{3}{2} \frac{k_B T_C}{S(S+1)} \frac{1}{z} \quad \text{or} \quad A = \frac{3}{2} \frac{k_B T_C S}{a(S+1)} \frac{n}{z}. \quad (17)$$

The second equation follows from the first one by replacing J with the relation (15). Here z is the number of nearest neighbors ($z = 6, 8, 12,$ and 12 for simple cubic, body centered cubic, face centered cubic, and hexagonal closed packed lattices, respectively) and $k_B = 1.3807 \times 10^{-23}$ J/K is Boltzmann's constant. The use of (17) together with (15) underestimates the exchange constant

by more than a factor of 2 [21]. Alternatively one can use the temperature dependence of the magnetization as arising from the spin wave theory

$$M_s(T) = M_s(0)(1 - CT^{3/2}). \quad (18)$$

Equation (18) is valid for low temperatures. From the measured temperature dependence $M_s(T)$ the constant C can be determined. Then the exchange integral [21, 22] and the exchange constant can be calculated from C as follows

$$J = \left(\frac{0.0587}{nSC}\right)^{2/3} \frac{k_B}{2S} \text{ or } A = \left(\frac{0.0587}{n^2S^2C}\right)^{2/3} \frac{k_B}{2a}. \quad (19)$$

This method was used by Talagala and co-workers [23]. They measured the temperature dependence of the saturation magnetization in NiCo films to determine the exchange constant as function of the Co content. The exchange constant can also be evaluated from the spin wave dispersion relation (see Chapter Spin Waves) which can be measured by inelastic neutron scattering, ferromagnetic resonance, or Brillouin light scattering [24]. The exchange integral [22] and the exchange constant are related to the spin wave stiffness constant, D , via the following relations

$$J = \frac{D}{2} \frac{1}{Sa^2} \text{ or } A = \frac{D}{2} NS \quad (20)$$

For the evaluation of the exchange constant we can use $S = M_s(0)/(Ng\mu_B)$ [25] for the spin quantum number in equations (17), (19), and (20). This gives the relation between the exchange constant, A , and the spin wave stiffness constant, D ,

$$A = \frac{DM_s(0)}{2g\mu_B}, \quad (21)$$

when applied to (20). Using neutron Brillouin scattering Ono and co-workers [26] measured the spin wave dispersion in a polycrystalline $\text{Nd}_2\text{Fe}_{14}\text{B}$ magnet, in order to determine its exchange constant.

Ferromagnetic exchange interactions keep the magnetization uniform. Depending on the sample geometry external fields may lead to a locally confined non-uniform magnetization. Probing the magnetization twist experimentally and comparing the result with a the computed equilibrium magnetic state (see Sect. 5) is an alternative method to determine the exchange constant. The measured data is fitted to the theoretical model whereby the exchange constant is a free parameter. Smith and co-workers [27] measured the anisotropic magnetoresistance to probe the fanning of the magnetization in a thin permalloy film from which its exchange constant was calculated. Eyrich and coworkers [24] measured the field dependent magnetization, $M(H)$, of a trilayer structure in which two ferromagnetic films are coupled antiferromagnetically. The $M(H)$ curve probes the magnetization twist within the two ferromag-

nets. Using this method the exchange constant of Co alloyed with various other elements was measured [24].

The interplay between the effects of ferromagnetic exchange coupling, magnetostatic interactions, and the magnetocrystalline anisotropy leads to the formation of domain patterns (for details on domain structures see Chapter Domains). With magnetic imaging techniques the domain width, the orientation of the magnetization, and the domain wall width can be measured. These values can be also calculated using a micromagnetic model of the domain structure. By comparing the predicted values for the domain width with measured data Livingston [28, 29] estimated the exchange constant of the hard magnetic materials SmCo_5 and $\text{Nd}_2\text{Fe}_{14}\text{B}$. This method can be improved by comparing more than one predicted quantity with measured data. Newnham and co-workers [30] measured the domain width, the orientation of the magnetization in the domain, and the domain wall width in foils of $\text{Nd}_2\text{Fe}_{14}\text{B}$. By comparing the measured values with the theoretical predictions they estimated the exchange constant of $\text{Nd}_2\text{Fe}_{14}\text{B}$.

Input for micromagnetic simulations: The high temperature behavior of permanent magnets is of outmost importance for the applications of permanent magnets in the hybrid or electric vehicles. For computation of the coercive field by micromagnetic simulations the exchange constant is needed as input parameter. Values for $A(T)$ may be obtained from the room temperature value of $A(300\text{ K})$ and $M_s(T)$. Applying (16) gives $A(T) = A(300\text{ K}) \times [M_s(T)/M_s(300\text{ K})]^2$.

3.3 Magnetostatics

We now consider the energy of the magnet in an external field produced by stationary currents and the energy of the magnet in the field produced by the magnetization of the magnet. The latter field is called demagnetizing field. In micromagnetics these fields can be treated statically if eddy currents are neglected. In magnetostatics we have no time dependent quantities. In the presence of a stationary magnetic current Maxwell's equations reduce to [31]

$$\nabla \times \mathbf{H} = \mathbf{j} \quad (22)$$

$$\nabla \cdot \mathbf{B} = 0 \quad (23)$$

Here \mathbf{B} is the magnetic induction or magnetic flux density, \mathbf{H} is the magnetic field, and \mathbf{j} is the current density. The charge density fulfills $\nabla \cdot \mathbf{j} = 0$ which expresses the conservation of electric charge. We now have the freedom to split the magnetic field into its solenoidal and nonrotational part

$$\mathbf{H} = \mathbf{H}_{\text{ext}} + \mathbf{H}_{\text{demag}}. \quad (24)$$

By definition we have

$$\nabla \cdot \mathbf{H}_{\text{ext}} = 0, \quad (25)$$

$$\nabla \times \mathbf{H}_{\text{demag}} = 0. \quad (26)$$

Using (22) and (24) we see that the external field, \mathbf{H}_{ext} , results from the current density (Ampere's law)

$$\nabla \times \mathbf{H}_{\text{ext}} = \mathbf{j}. \quad (27)$$

On a macroscopic length scale the relation between the magnetic induction and the magnetic field is expressed by

$$\mathbf{B} = \mu \mathbf{H}, \quad (28)$$

where μ is the permeability of the material. Equation (28) is used in magnetostatic field solvers [32] for the design of magnetic circuits. In these simulations the permeability describes the response of the material to the magnetic field. Micromagnetics describes the material on a much finer length scale. In micromagnetics we compute the local distribution of the magnetization as function of the magnetic field. This is the response of the system to (an external) field. Indeed, the permeability can be derived from micromagnetic simulations [33]. For the calculation of the demagnetizing field, we can treat the magnetization as fixed function of space. Instead of (28) we use

$$\mathbf{B} = \mu_0 (\mathbf{H} + \mathbf{M}). \quad (29)$$

The energy of the magnet in the external field, \mathbf{H}_{ext} , is the Zeeman energy. The energy of the magnet in the demagnetizing field, $\mathbf{H}_{\text{demag}}$, is called magnetostatic energy.

3.4 Zeeman energy

The energy of a magnetic dipole moment, $\boldsymbol{\mu}$, in an external magnetic induction \mathbf{B}_{ext} is $-\boldsymbol{\mu} \cdot \mathbf{B}_{\text{ext}}$. We use $\mathbf{B}_{\text{ext}} = \mu_0 \mathbf{H}_{\text{ext}}$ and sum over all local magnetic moments at positions \mathbf{x}_i of the ferromagnet. The sum,

$$E_{\text{ext}} = -\mu_0 \sum_i \boldsymbol{\mu}_i \cdot \mathbf{H}_{\text{ext}}, \quad (30)$$

is the interaction energy of the magnet with the external field. To obtain the Zeeman energy in a continuum model we introduce the magnetization $\mathbf{M} = N \boldsymbol{\mu}$, define the volume per atom, $V_i = 1/N$, and replace the sum with an integral. We obtain

$$E_{\text{ext}} = -\mu_0 \sum_i (\mathbf{M} \cdot \mathbf{H}_{\text{ext}}) V_i \rightarrow -\mu_0 \int_V (\mathbf{M} \cdot \mathbf{H}_{\text{ext}}) dV. \quad (31)$$

Using (6) we express the Zeeman energy in terms of the unit vector of the magnetization

$$E_{\text{ext}} = - \int_V \mu_0 M_s (\mathbf{m} \cdot \mathbf{H}_{\text{ext}}) dV. \quad (32)$$

3.5 Magnetostatic energy

The magnetostatic energy is also called dipolar interaction energy. In a crystal each moment creates a dipole field and each moment is exposed to the magnetic field created by all other dipoles. Therefore magnetostatic interactions are long range. The magnetostatic energy cannot be represented as a volume integral over the magnet of an energy density dependent on only local quantities.

3.5.1 Demagnetizing field as sum of dipolar fields

The total magnetic field at point \mathbf{x}_i , which is created by all the other magnetic dipoles, is the sum over the dipole fields from all moments $\boldsymbol{\mu}_j = \boldsymbol{\mu}(\mathbf{x}_j)$

$$\mathbf{H}_{\text{dip}}(\mathbf{x}_i) = \frac{1}{4\pi} \sum_{j \neq i} \left[3 \frac{(\boldsymbol{\mu}_j \cdot \mathbf{r}_{ij}) \mathbf{r}_{ij}}{r_{ij}^5} - \frac{\boldsymbol{\mu}_j}{r_{ij}^3} \right]. \quad (33)$$

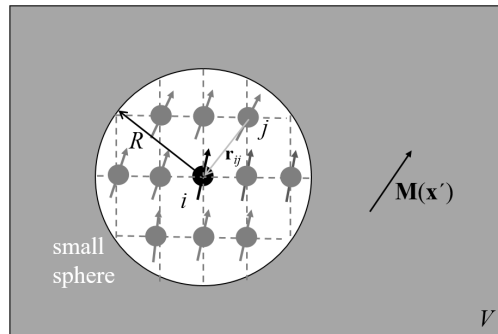


Fig. 2 Computation of the total magnetostatic field at point atom i . The near field is evaluated by a direct sum over all dipoles in the small sphere. The atomic moments outside the sphere are replaced by a continuous magnetization which produces the far field acting on i .

The vectors $\mathbf{r}_{ij} = \mathbf{x}_i - \mathbf{x}_j$ connect the source points with the field point. The distance between a source point and a field point is $r_{ij} = |\mathbf{r}_{ij}|$. In order to obtain a continuum expression for the field we split the sum (33) in two parts. The contribution to the field from moments that are far from \mathbf{x}_i will not depend strongly on their exact position at the atomic level. Therefore we can describe them by a continuous magnetization and replace the sum with an integral. For moments $\boldsymbol{\mu}_j$ which are located within a small sphere with radius R around \mathbf{x}_i we keep the sum. Thus we split the dipole field into two parts [34]:

$$\mathbf{H}_{\text{dip}}(\mathbf{x}_i) = \mathbf{H}_{\text{near}} + \mathbf{H}_{\text{demag}}. \quad (34)$$

Here

$$\mathbf{H}_{\text{near}}(\mathbf{x}_i) = \frac{1}{4\pi} \sum_{r_{ij} < R} \left[3 \frac{(\boldsymbol{\mu}_j \cdot \mathbf{r}_{ij}) \mathbf{r}_{ij}}{r_{ij}^5} - \frac{\boldsymbol{\mu}_j}{r_{ij}^3} \right] \quad (35)$$

is the contribution of the sum of the dipoles within the sphere (see Fig. 2). For the dipoles outside the sphere we use a continuum approximation. Introducing the magnetic dipole element $\mathbf{M}dV'$, we can replace the sum in (33) with an integral for $r_{ij} \geq R$

$$\mathbf{H}_{\text{demag}}(\mathbf{x}) = \frac{1}{4\pi} \int_{V^*} \left[3 \frac{(\mathbf{M}(\mathbf{x}') \cdot (\mathbf{x} - \mathbf{x}')) (\mathbf{x} - \mathbf{x}')}{|\mathbf{x} - \mathbf{x}'|^5} - \frac{\mathbf{M}(\mathbf{x}')}{|\mathbf{x} - \mathbf{x}'|^3} \right] dV'. \quad (36)$$

The integral excludes the small sphere. The integral is over V^* , the volume of the magnet without a small sphere around the field point \mathbf{x} .

The sum in (35) is the contribution of the dipoles inside the sphere to the total magnetostatic field. The corresponding energy term is local. It can be expressed as an integral of an energy density that depends only on local quantities [34]. The term depends on the symmetry of the lattice and has the same form as the crystalline anisotropy. Therefore it is included in the anisotropy energy. When the anisotropy constants in (58) are determined experimentally, they already include the contribution owing to dipolar interactions.

3.5.2 Magnetic scalar potential

The demagnetizing field is nonrotational. Therefore we can write the demagnetizing field as gradient of a scalar potential

$$\mathbf{H}_{\text{demag}} = -\nabla U. \quad (37)$$

Applying $-\nabla$ to

$$U(\mathbf{x}) = -\frac{1}{4\pi} \int_{V^*} \mathbf{M}(\mathbf{x}') \cdot \frac{\mathbf{x} - \mathbf{x}'}{|\mathbf{x} - \mathbf{x}'|^3} dV'. \quad (38)$$

gives (36). In computational micromagnetics it is beneficial to work with effective magnetic volume charges, $\rho_m = -\nabla' \cdot \mathbf{M}(\mathbf{x}')$, and effective magnetic surface charges, $\sigma_m = \mathbf{M}(\mathbf{x}') \cdot \mathbf{n}$. Using

$$\frac{\mathbf{x} - \mathbf{x}'}{|\mathbf{x} - \mathbf{x}'|^3} = -\nabla \frac{1}{|\mathbf{x} - \mathbf{x}'|} \text{ and } \nabla \frac{1}{|\mathbf{x} - \mathbf{x}'|} = -\nabla' \frac{1}{|\mathbf{x} - \mathbf{x}'|} \quad (39)$$

we obtain

$$U(\mathbf{x}) = \frac{1}{4\pi} \int_{V^*} \mathbf{M}(\mathbf{x}') \cdot \nabla' \frac{1}{|\mathbf{x} - \mathbf{x}'|} dV'. \quad (40)$$

Now we shift the ∇' operator from $1/|\mathbf{x} - \mathbf{x}'|$ to \mathbf{M} . We use

$$\nabla' \cdot \frac{\mathbf{M}(\mathbf{x}')}{|\mathbf{x} - \mathbf{x}'|} = \frac{\nabla' \cdot \mathbf{M}(\mathbf{x}')}{|\mathbf{x} - \mathbf{x}'|} + \mathbf{M}(\mathbf{x}') \cdot \nabla' \frac{1}{|\mathbf{x} - \mathbf{x}'|}, \quad (41)$$

apply Gauss'Ä theorem, and obtain [31]

$$U(\mathbf{x}) = \frac{1}{4\pi} \int_{V^*} \frac{\rho_m(\mathbf{x}')}{|\mathbf{x} - \mathbf{x}'|} dV' + \frac{1}{4\pi} \oint_{\partial V^*} \frac{\sigma_m(\mathbf{x}')}{|\mathbf{x} - \mathbf{x}'|} dS'. \quad (42)$$

3.5.3 Magnetostatic energy

For computing the magnetostatic energy there is no need to take into account (35). The near field is already included in the crystal anisotropy energy. We now compute the energy of each magnetic moment $\boldsymbol{\mu}_i$ in the field $\mathbf{H}_{\text{demag}}(\mathbf{x}_i)$ from the surrounding magnetization. Summing the energy of all over all atoms we get the magnetostatic energy of the magnet

$$E_{\text{demag}} = -\frac{\mu_0}{2} \sum_i \boldsymbol{\mu}_i \cdot \mathbf{H}_{\text{demag}}(\mathbf{x}_i). \quad (43)$$

The factor 1/2 avoids counting each pair of atoms twice. Similar to the procedure for the exchange and Zeeman energy we replace the sum with an integral

$$E_{\text{demag}} = -\frac{\mu_0}{2} \int_V \mathbf{M} \cdot \mathbf{H}_{\text{demag}} = -\frac{1}{2} \int_V \mu_0 M_s (\mathbf{m} \cdot \mathbf{H}_{\text{demag}}) dV. \quad (44)$$

Alternatively, the magnetostatic energy can be expressed in terms of a magnetic scalar potential and effective magnetic charges. We start from (44), replace $\mathbf{H}_{\text{demag}}$ by $-\nabla U$, and apply Gauss'Ä theorem on $\nabla \cdot (\mathbf{M}U)$ to obtain

$$E_{\text{demag}} = \frac{\mu_0}{2} \int_V \rho_m U dV + \frac{\mu_0}{2} \oint_{\partial V} \sigma_m U dS. \quad (45)$$

Equation (45) is widely used in numerical micromagnetics. Its direct variation (see Sect. 5) with respect to \mathbf{M} gives the cell averaged demagnetizing field. This method was introduced in numerical micromagnetics by LaBonte [35] and Schabes and Aharoni [36]. For discretization with piecewise constant magnetization only the surface integrals remain.

In a uniformly magnetized spheroid the demagnetizing field is antiparallel to the magnetization. The demagnetizing field is

$$\mathbf{H}_{\text{demag}} = -N\mathbf{M}, \quad (46)$$

where N is the demagnetizing factor. For a sphere the demagnetizing factor is $1/3$. Using (44) we find

$$E_{\text{demag}} = \frac{\mu_0}{2}NM_s^2V \quad (47)$$

for the magnetostatic energy of a uniformly magnetized spheroid with volume V . In a cuboid or polyhedral particle the demagnetizing field is nonuniform. However we still can apply (47) when we use a volume averaged demagnetizing factor which is obtained from a volume averaged demagnetizing field. Interestingly the volume averaged demagnetizing factor for a cube is $1/3$ the same value as for the sphere. For a general rectangular prism Aharoni [37] calculated the volume averaged demagnetizing factor. A convenient calculation tool for the demagnetizing factor, which uses Aharoni's equation, is given on the *Magpar* website [38]. A simple approximate equation for the demagnetizing factor of a square prism with dimensions $l \times l \times pl$ is [39]

$$N = \frac{1}{2p + 1}, \quad (48)$$

where p is the aspect ratio and N is the demagnetizing factor along the edge with length pl .

3.5.4 Magnetostatic boundary value problem

Equation (42) is the solution of the magnetostatic boundary value problem, which can be derived from Maxwell's equations as follows. From (23) and (29) the following equation holds for the demagnetizing field

$$\nabla \cdot \mathbf{H}_{\text{demag}} = -\nabla \cdot \mathbf{M}. \quad (49)$$

Plugging (37) into (49) we obtain a partial differential equation for the scalar potential

$$\nabla^2 U = \nabla \cdot \mathbf{M}. \quad (50)$$

Equation (50) holds inside the magnet. Outside the magnet $\mathbf{M} = 0$ and we have

$$\nabla^2 U = 0. \quad (51)$$

At the magnet's boundary the following interface conditions [31] hold

$$U^{(\text{in})} = U^{(\text{out})}, \quad (52)$$

$$\left(\nabla U^{(\text{in})} - \nabla U^{(\text{out})} \right) \cdot \mathbf{n} = \mathbf{M} \cdot \mathbf{n}, \quad (53)$$

where \mathbf{n} denotes the surface normal. The first condition follows from the continuity of the component of \mathbf{H} parallel to the surface (or $\nabla \times \mathbf{H} = 0$). The second condition follows from the continuity of the component of \mathbf{B} normal to the surface (or $\nabla \cdot \mathbf{B} = 0$). Assuming that the scalar potential is regular at infinity,

$$U(\mathbf{x}) \leq C \frac{1}{|\mathbf{x}|} \text{ for } |\mathbf{x}| \text{ large enough and constant } C > 0 \quad (54)$$

the solution of equations (50) to (53) is given by (42). Formally the integrals in (42) are over the volume, V^* , and the surface, ∂V^* , of the magnet without a small sphere surrounding the field point. The transition from $V^* \rightarrow V$ adds a term the term $-\mathbf{M}/3$ to the field and thus shifts the energy by a constant which is proportional to M_s^2 . This is usually done in micromagnetics [34].

The above set of equations for the magnetic scalar potential can also be derived from a variational principle. Brown [16] introduced an approximate expression

$$E'_{\text{demag}} = \mu_0 \int_V \mathbf{M} \cdot \nabla U' dV - \frac{\mu_0}{2} \int_V (\nabla U')^2 dV \quad (55)$$

for the magnetostatic energy, E_{demag} . For any magnetization distribution $\mathbf{M}(\mathbf{x})$ the following equation holds

$$E_{\text{demag}}(\mathbf{M}) \geq E'_{\text{demag}}(\mathbf{M}, U'), \quad (56)$$

where U' is arbitrary function which is continuous in space and regular at infinity [16]. A proof of (56) is given by Asselin and Thiele [40]. If maximized the functional E'_{demag} makes U' equal to the magnetic scalar potential owing to \mathbf{M} . Then the equal sign holds and E'_{demag} reduces to the usual magnetostatic energy E_{demag} . Equation (55) is used in finite element micromagnetics for the computation of the magnetic scalar potential. The Euler-Lagrange equation of (55) with respect to U' gives the magnetostatic boundary value problem (50) to (53) [40].

3.5.5 Examples

Magnetostatic energy in micromagnetic software: For physicists and software engineers developing micromagnetic software there are several options to implement magnetostatic field computation. The choice depends on the dis-

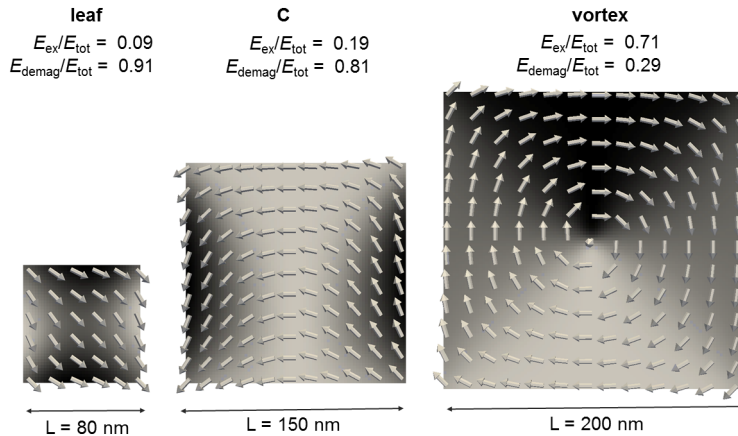


Fig. 3 Computed magnetization patterns for a soft magnetic square element ($K_1 = 0$, $\mu_0 M_s = 1$ T, $A = 10$ pJ/m, mesh size $h = 0.56\sqrt{A/(\mu_0 M_s^2)} = 2$ nm) as function of element size L . The dimensions are $L \times L \times 6$ nm³. The system was relaxed multiple times from an initial state with random magnetization. The lowest energy states are the leaf state, the C-state, and the vortex state for $L = 80$ nm, $L = 150$ nm, and $L = 200$ nm, respectively. For each state the relative contributions of the exchange energy and the magnetostatic energy to the total energy are given.

cretization scheme, the numerical methods used, and the hardware. Finite difference solvers including *OOMMF* [41], *MuMax3* [42], and *FIDIMAG* [43] use (45) to compute the magnetostatic energy and the cell averaged demagnetizing field. For piecewise constant magnetization only the surface integrals over the surfaces of the computational cells remain. *MicroMagnum* [44] uses (42) to evaluate the magnetic scalar potential. The demagnetizing field is computed from the potential by a finite difference approximation. This method shows a higher speed up on Graphics Processor Units [45] though its accuracy is slightly less. Finite element solvers compute the magnetic scalar potential and build its gradient. *Magpar* [46], *Nmag* [47], and *magnum.fe* [48] solve the partial differential equations (50) to (53). *FastMag* [49], a finite element solver, directly integrates (42). Finite difference solvers apply the Fast Fourier Transforms for the efficient evaluation of the involved convolutions. Finite element solvers often use hierarchical clustering techniques for the evaluation of integrals.

Magnetic state of nano-elements: From (45) we see that the magnetostatic energy tends to zero if the effective magnetic charges vanish. This is known as pole avoidance principle [34]. In large samples where the magnetostatic energy dominates over the exchange energy the lowest energy configurations are such that $\nabla \cdot \mathbf{M}$ in the volume and $\mathbf{M} \cdot \mathbf{n}$ on the surface tend to zero. The magnetization is aligned parallel to the boundary and may show a vortex. These patterns are known as flux closure states. In small samples the expense

of exchange energy for the formation of a closure state is too high. As a compromise the magnetization bends towards the surface near the edges of the sample. Depending on the size the leaf state [50] or the C-state [51] or the vortex state have the lowest energy. Fig. 3 shows the different magnetization patterns that can form in thin film square elements. The results show that with increasing element size the relative contribution of the magnetostatic energy, $F_{\text{demag}}/(F_{\text{ex}} + F_{\text{demag}})$ decreases. All micromagnetic examples in this chapter are simulated using *FIDIMAG* [43]. Code snippets for each example are given in the appendix.

3.6 Crystal anisotropy energy

The magnetic properties of a ferromagnetic crystal are anisotropic. Depending on the orientation of the magnetic field with respect to the symmetry axes of the crystal the $M(H)$ curve reaches the saturation magnetization, M_s , at low or high field values. Thus easy directions in which saturation is reached in a low field and hard directions in which high saturation requires a high field are defined. Fig 4 shows the magnetization curve of a uniaxial material with strong crystal anisotropy in the easy and hard direction. The initial state is a two domain state with the magnetization of the domains parallel to the easy axis. The snap shots of the magnetic states show that domain wall motion occurs along the easy axis and rotation of the magnetization occurs along the hard axis.

The crystal anisotropy energy is the work done by the external field to move the magnetization away from a direction parallel to the easy axis. The functional form of the energy term can be obtained phenomenologically. The energy density, $e_{\text{ani}}(\mathbf{m})$, is expanded in a power series in terms of the direction cosines of the magnetization. Crystal symmetry is used to decrease the number of coefficients. The series is truncated after the first two non-constant terms.

3.6.1 Cubic anisotropy

Let \mathbf{a} , \mathbf{b} , and \mathbf{c} be the unit vectors along the axes of a cubic crystal. The crystal anisotropy energy density of a cubic crystal is

$$\begin{aligned}
 e_{\text{ani}}(\mathbf{m}) = & K_0 + \\
 & K_1 [(\mathbf{a} \cdot \mathbf{m})^2(\mathbf{b} \cdot \mathbf{m})^2 + (\mathbf{b} \cdot \mathbf{m})^2(\mathbf{c} \cdot \mathbf{m})^2 + (\mathbf{c} \cdot \mathbf{m})^2(\mathbf{a} \cdot \mathbf{m})^2] + \\
 & K_2 [(\mathbf{a} \cdot \mathbf{m})^2(\mathbf{b} \cdot \mathbf{m})^2(\mathbf{c} \cdot \mathbf{m})^2] + \dots
 \end{aligned}
 \tag{57}$$

The anisotropy constants K_0 , K_1 , and K_2 are a function of temperature. The first term is independent of \mathbf{m} and thus can be dropped since only the change of the energy with respect to the direction of the magnetization is of interest.

3.6.2 Uniaxial anisotropy

In hexagonal or tetragonal crystals the crystal anisotropy energy density is usually expressed in terms of $\sin^2 \theta$, where θ is the angle between the c-axis and the magnetization. The crystal anisotropy energy of a hexagonal or tetragonal crystal is

$$e_{\text{ani}}(\mathbf{m}) = K_0 + K_1 \sin^2(\theta) + K_2 \sin^4(\theta) + \dots \quad (58)$$

In numerical micromagnetics it is often more convenient to use

$$e'_{\text{ani}}(\mathbf{m}) = -K_1(\mathbf{c} \cdot \mathbf{m})^2 + \dots \quad (59)$$

as expression for a uniaxial crystal anisotropy energy density. Here we used the identity $\sin^2(\theta) = 1 - (\mathbf{c} \cdot \mathbf{m})^2$, dropped two constant terms, namely K_0 and K_1 , and truncated the series. When keeping only the terms which are quadratic in \mathbf{m} , the crystal anisotropy energy can be discretized as quadratic form involving only a geometry dependent matrix.

The crystalline anisotropy energy is

$$E_{\text{ani}} = \int_V e_{\text{ani}}(\mathbf{m}) dV, \quad (60)$$

whereby the integral is over the volume, V , of the magnetic body.

3.6.3 Anisotropy field

An important material parameter, which is commonly used, is the anisotropy field, H_K . The anisotropy field is a fictitious field that mimics the effect of the crystalline anisotropy. If the magnetization vector rotates out of the easy axis the crystalline anisotropy creates a torque that brings \mathbf{M} back into the easy direction. The anisotropy field is parallel to the easy direction and its magnitude is such that for deviations from the easy axis the torque on \mathbf{M} is the same as the torque by the crystalline anisotropy. If the energy depends on the angle, θ , of the magnetization with respect to an axis, the torque, T , on the magnetization is the derivative of the energy density, e , with respect to the angle [20]

$$T = \frac{\partial e}{\partial \theta}. \quad (61)$$

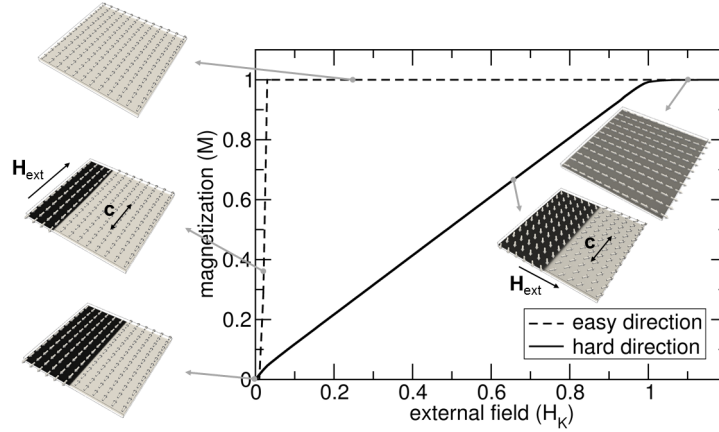


Fig. 4 Initial magnetization curves with the field applied in the easy direction (dashed line) and the hard direction (solid line) computed for a uniaxial hard magnetic material ($\text{Nd}_2\text{Fe}_{14}\text{B}$ at room temperature: $K_1 = 4.9 \text{ MJ/m}^3$, $\mu_0 M_s = 1.61 \text{ T}$, $A = 8 \text{ pJ/m}$, the mesh size is $h = 0.86 \sqrt{A/K_1} = 1.1 \text{ nm}$). The magnetization component parallel to the field direction is plotted as a function of the external field. The field is given in units of H_K . The sample shape is thin platelet with the easy axis in the plane of the film. The sample dimensions are $200 \times 200 \times 10 \text{ nm}^3$. The insets show snap shots of the magnetization configuration along the curves. The initial state is the two domain state shown at the lower left of the figure.

Let θ be a small angular deviation of \mathbf{M} from the easy direction. The energy density of the magnetization in the anisotropy field is

$$e_K = -\mu_0 M_s H_K \cos(\theta) \quad (62)$$

the associated torque is

$$T_K = \mu_0 M_s H_K \sin(\theta) \approx \mu_0 M_s H_K \theta. \quad (63)$$

For the crystalline anisotropy energy density

$$e_{\text{ani}} = K_1 \sin^2(\theta) \quad (64)$$

the torque towards the easy axis is

$$T_{\text{ani}} = 2K_1 \sin(\theta) \cos(\theta) = K_1 \sin(2\theta) \approx 2K_1 \theta. \quad (65)$$

From the definition of the anisotropy field, namely $T_K = T_{\text{ani}}$, we get

$$H_K = \frac{2K_1}{\mu_0 M_s} \quad (66)$$

Anisotropy field, easy and hard axis loops: K_1 and – depending on the material to be studied – K_2 are input parameters for micromagnetic simulation. The anisotropy constants can be measured by fitting a calculated magnetization curve to experimental data. Fig. 4 shows the magnetization curves of a uniaxial material computed by micromagnetic simulations. For simplicity we neglected K_2 and described the crystalline anisotropy with (59). The $M(H)$ along the hard direction is almost a straight line until saturation where $M(H) = M_s$. Saturation is reached when $H = H_K$.

The above numerical result can be found theoretically. A field is applied perpendicular to the easy direction. The torque created by the field, tends to increase the angle, θ , between the magnetization and the easy axis. The torque asserted by the crystalline anisotropy returns the magnetization towards the easy direction. We set the total torque to zero to get the equilibrium condition

$$-\mu_0 M_s H \cos(\theta) + 2K_1 \sin(\theta) \cos(\theta) = 0$$

The value of H that makes \mathbf{M} parallel to the field is reached when $\sin(\theta) = 1$. This gives $H = 2K_1/(\mu_0 M_s)$. If higher anisotropy constants are taken into account the field that brings \mathbf{M} into the hard axis is $H = (2K_1 + 4K_2)/(\mu_0 M_s)$.

3.7 Magnetoelastic and magnetostrictive energy terms

When the atom positions of a magnet are changed relative to each other the crystalline anisotropy varies. Owing to magnetoelastic coupling a deformation produced by an external stress makes certain directions to be energetically more favorable. Reversely, the magnet will deform in order to minimize its total free energy when magnetized in certain direction.

3.7.1 Spontaneous magnetostrictive deformation

Most generally the spontaneous magnetostrictive deformation is expressed by the symmetric tensor strain ε_{ij}^0 as

$$\varepsilon_{ij}^0 = \sum_{kl} \lambda_{ijkl} \alpha_k \alpha_l, \quad (67)$$

where λ_{ijkl} is the tensor of magnetostriction constants. Measurements of the relative change of length along certain directions owing to saturation of the crystal in direction $\boldsymbol{\alpha} = (\alpha_1, \alpha_2, \alpha_3)$ gives the magnetostriction constants. For a cubic material the following relation holds

$$\varepsilon_{ii}^0 = \frac{3}{2}\lambda_{100}\left(\alpha_i^2 - \frac{1}{3}\right) \quad (68)$$

$$\varepsilon_{ij}^0 = \frac{3}{2}\lambda_{111}\alpha_i\alpha_j \quad \text{for } i \neq j. \quad (69)$$

The magnetostriction constants λ_{100} and λ_{111} are defined as follows: λ_{100} is the relative change in length measured along [100] owing to saturation of the crystal in [100]; similarly λ_{111} is the relative change in length measured along [111] owing to saturation of the crystal in [111]. The term with $1/3$ in (68) results from the definition of the spontaneous deformation with respect to a demagnetized state with the averages $\langle\alpha_i^2\rangle = 1/3$ and $\langle\alpha_i\alpha_j\rangle = 0$.

3.7.2 Magnetoelastic coupling energy

All energy terms discussed in the previous sections can depend on deformations. The most important change of energy with strain arises from the crystal anisotropy energy. Thus the crystal anisotropy energy is a function of the magnetization and the deformation of the lattice. We express the magnetization direction in terms of the direction cosines of the magnetization $\alpha_1 = \mathbf{a} \cdot \mathbf{m}$, $\alpha_2 = \mathbf{b} \cdot \mathbf{m}$, and $\alpha_3 = \mathbf{c} \cdot \mathbf{m}$ (\mathbf{a} , \mathbf{b} , and \mathbf{c} are the unit lattice vectors) and the deformation in terms of the symmetric strain tensor ε_{ij} to obtain

$$e_{\text{ani}} = e_{\text{ani}}(\alpha_i, \varepsilon_{ij}). \quad (70)$$

A Taylor expansion of (70)

$$e_{\text{ani}} = e_{\text{ani}}(\alpha_i, 0) + \sum_{ij} \frac{\partial e_{\text{ani}}(\alpha_i, 0)}{\partial \varepsilon_{ij}} \varepsilon_{ij} \quad (71)$$

gives the change of the energy density owing to the strain ε_{ij} . Owing to symmetry the expansion coefficients $\partial e_{\text{ani}}(\alpha_i, 0)/\partial \varepsilon_{ij}$ do not depend on the sign of the magnetization vector and thus are proportional to $\alpha_i\alpha_j$. The second term on the right hand side of (71) is the change of the crystal anisotropy energy density with deformation. This term is the magnetoelastic coupling energy density. Using $\sum_{ij} B_{ijkl}\alpha_i\alpha_j$ as expansion coefficients we obtain

$$e_{\text{me}} = \sum_{ij} \sum_{kl} B_{ijkl}\alpha_i\alpha_j\varepsilon_{kl}, \quad (72)$$

where B_{ijkl} is the tensor of the magnetoelastic coupling constants. For cubic symmetry the magnetoelastic coupling energy density is

$$e_{\text{me, cubic}} = B_1(\varepsilon_{11}\alpha_1^2 + \varepsilon_{22}\alpha_2^2 + \varepsilon_{33}\alpha_3^2) + 2B_2(\varepsilon_{23}\alpha_2\alpha_3 + \varepsilon_{13}\alpha_1\alpha_3 + \varepsilon_{12}\alpha_1\alpha_2) + \dots \quad (73)$$

with the magnetoelastic coupling constants $B_1 = B_{1111}$ and $B_2 = B_{2323}$. Equation 72 describes change of the energy density owing to the interaction of magnetization direction and deformation. The magnetoelastic coupling constants can be derived from the ab-initio computation of the crystal anisotropy energy as function of strain [52]. Experimentally the magnetoelastic coupling constants can be obtained from the measured magnetostriction constants.

When magnetized in a certain direction the magnet tends to deform in a way that minimizes the sum of the magnetoelastic energy density, e_{me} , and of the elastic energy density of the crystal, e_{el} . The elastic energy density is a quadratic function of the strain

$$e_{el} = \frac{1}{2} \sum_{ij} \sum_{kl} c_{ijkl} \varepsilon_{ij} \varepsilon_{kl}, \quad (74)$$

where c_{ijkl} is the elastic stiffness tensor. For cubic crystals the elastic energy is

$$\begin{aligned} e_{el,cubic} = & \frac{1}{2} c_{1111} (\varepsilon_{11}^2 + \varepsilon_{22}^2 + \varepsilon_{33}^2) + \\ & c_{1122} (\varepsilon_{11} \varepsilon_{22} + \varepsilon_{22} \varepsilon_{33} + \varepsilon_{33} \varepsilon_{11}) + \\ & 2c_{2323} (\varepsilon_{12}^2 + \varepsilon_{23}^2 + \varepsilon_{31}^2). \end{aligned} \quad (75)$$

Minimizing $e_{me} + e_{el}$ with respect to ε_{ij} under fixed α_i gives the equilibrium strain or spontaneous magnetostrictive deformation

$$\varepsilon_{ij}^0 = \varepsilon_{ij}^0(B_{ijkl}, c_{ijkl}). \quad (76)$$

in terms of the magnetoelastic coupling constants and the elastic stiffness constants. Comparison of the coefficients in (76) and the experimental relation (67) allows to express the magnetoelastic coupling coefficients in terms of the elastic stiffness constants and the magnetostriction constants. For cubic symmetry the magnetoelastic coupling constants are

$$B_1 = -\frac{3}{2} \lambda_{100} (c_{1111} - c_{1122}) \quad (77)$$

$$B_2 = -3 \lambda_{111} c_{1212}. \quad (78)$$

3.7.3 External stress

A mechanical stress of nonmagnetic origin will have an effect on the magnetization owing to a change of magnetoelastic coupling energy. The magnetoelastic coupling energy density owing to an external stress σ^{ext} is [53]

$$e_{me} = - \sum_{ij} \sigma_{ij}^{\text{ext}} \varepsilon_{ij}^0 \quad (79)$$

For cubic symmetry this gives [20]

$$e_{\text{me,cubic}} = -\frac{3}{2}\lambda_{100}(\sigma_{11}\alpha_1^2 + \sigma_{22}\alpha_2^2 + \sigma_{33}\alpha_3^2) - 3\lambda_{111}(\sigma_{12}\alpha_1\alpha_2 + \sigma_{23}\alpha_2\alpha_3 + \sigma_{31}\alpha_3\alpha_1) \quad (80)$$

The above results can be derived from the strain induced by the external stress which is

$$\varepsilon_{ij}^{\text{ext}} = \sum_{kl} s_{ijkl} \sigma_{kl}^{\text{ext}}, \quad (81)$$

where s_{ijkl} is the compliance tensor. Inserting (81) into (72) gives the magnetoelastic energy density owing to external stress. For an isotropic material, for example an amorphous alloy, we have only a single magnetostriction constant $\lambda_s = \lambda_{100} = \lambda_{111}$. For a stress σ along an axis of a unit vector \mathbf{a} the magnetoelastic coupling energy reduces to

$$e_{\text{me,isotropic}} = -\frac{3}{2}\lambda_s\sigma(\mathbf{a} \cdot \boldsymbol{\alpha})^2. \quad (82)$$

This is equation has a similar form as that for the uniaxial anisotropy energy density (59) with an anisotropy constant $K_{\text{me}} = 3\lambda_s\sigma/2$.

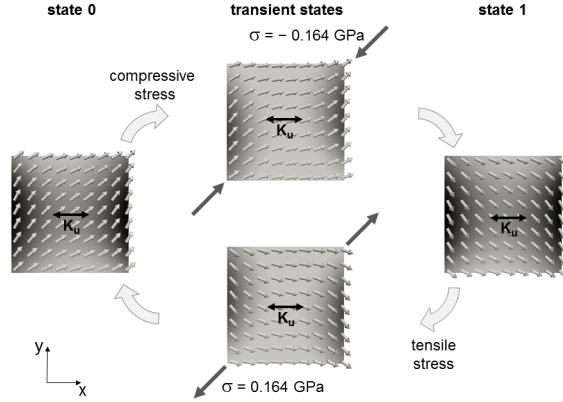


Fig. 5 Simulation of the stress-driven switching of a CoFeB nanoelement ($K_u = 1.32 \text{ kJ/m}^3$, $\mu_0 M_s = 1.29 \text{ T}$, $A = 15 \text{ pJ/m}$, $\lambda_s = 3 \times 10^{-5}$, mesh size $h = 0.59\sqrt{A/(\mu_0 M_s^2)} = 2 \text{ nm}$, the magnetostrictive self energy is neglected). The sample is a thin film element with dimensions $120 \times 120 \times 2 \text{ nm}^3$. The system switches from 0 to 1 by a compressive stress (-0.164 GPa) and from 1 to 0 by a tensile stress (0.164 GPa).

3.7.4 Magnetostrictive self energy

A nonuniform magnetization causes a nonuniform spontaneous deformation owing to (67). As a consequence different parts of the magnet do not fit together. To compensate this misfit an additional elastic deformation, $\varepsilon_{ij}^{\text{el}}$, will occur. The associated magnetostrictive self energy density is

$$e_{\text{magstr}} = \frac{1}{2} \sum_{ij} \sum_{kl} c_{ijkl} \varepsilon_{ij}^{\text{el}} \varepsilon_{kl}^{\text{el}}. \quad (83)$$

To compute $\varepsilon_{ij}^{\text{el}}$ we have to solve an elasticity problem. The total strain,

$$\varepsilon_{ij} = \varepsilon_{ij}^{\text{el}} + \varepsilon_{ij}^0, \text{SS} \quad (84)$$

can be derived from a displacement field, $\mathbf{u} = (u_1, u_2, u_3)$, according to [54]

$$\varepsilon_{ij} = \frac{1}{2} \left(\frac{\partial u_i}{\partial x_j} + \frac{\partial u_j}{\partial x_i} \right). \quad (85)$$

We start from a hypothetically undeformed, nonmagnetic nonmagnetic body. If magnetism is switched on ε_{ij}^0 causes a stress which we treat as virtual body forces. Once these forces are known the displacement field can be calculated as usual by linear elasticity theory. The situation is similar to magnetostatics where the demagnetizing field is calculated from effective magnetic charges. The procedure is as follows [55]. First we compute the the spontaneous magnetostrictive strain for a given magnetization distribution with (67) or in case of cubic symmetry with (68) and (69). Then we apply Hooke's law to compute the stress

$$\sigma_{ij}^0 = \sum_{kl} c_{ijkl} \varepsilon_{kl}^0 \quad (86)$$

owing to the spontaneous magnetostrictive strain. The stress is interpreted as virtual body force

$$f_i = - \sum_j \frac{\partial}{\partial x_j} \sigma_{ij}^0. \quad (87)$$

The forces enter the condition for mechanical equilibrium

$$\sum_j \frac{\partial}{\partial x_j} \sigma_{ij} = f_i \quad \text{with} \quad \sigma_{ij} = \sum_{kl} c_{ijkl} \varepsilon_{kl}. \quad (88)$$

Equations (85) to (88) lead to a systems of partial differential equations for the displacement field $\mathbf{u}(\mathbf{x})$. This is an auxiliary problem similar to the magnetostatic boundary value problem (see Sect. 3.5.4) which as to be solved for a given magnetization distribution.

Based on the above discussion we can identify two contributions to the total magnetic Gibbs free energy: The magnetoelastic coupling energy with an external stress

$$E_{\text{me}} = - \int_V \sum_{ij} \sigma_{ij}^{\text{ext}} \varepsilon_{ij}^0 dV \quad (89)$$

and the magnetostrictive self energy

$$E_{\text{magstr}} = \frac{1}{2} \int_V \sum_{ij} \sum_{kl} c_{ijkl} (\varepsilon_{ij} - \varepsilon_{ij}^0) (\varepsilon_{kl} - \varepsilon_{kl}^0) dV. \quad (90)$$

Artificial multiferroics: The magnetoelastic coupling becomes important in artificial multiferroic structures where ferromagnetic and piezoelectric elements are combined to achieve a voltage controlled manipulation of the magnetic state [56]. For example piezoelectric elements can create a strain on a magnetic tunnel junction of about 10^{-3} causing the magnetization to rotate by 90 degrees [57]. Breaking the symmetry by a stress induced uniaxial anisotropy the deterministic switching between two metastable states in square nano-element is possible as shown in Fig. (5).

4 Characteristic length scales

To obtain a qualitative understanding of equilibrium states it is helpful to consider the relative weight of the different energy terms towards the total Gibbs free energy. As shown in Fig. 3 the relative importance of the different energy terms changes with the size of the magnetic sample. We can see this most easily when we write the total Gibbs free energy

$$E_{\text{tot}} = E_{\text{ex}} + E_{\text{ext}} + E_{\text{demag}} + E_{\text{ani}} + E_{\text{me}} + E_{\text{magstr}}, \quad (91)$$

in dimensionless form. From the relative weight of the energy contributions in dimensionless form we will derive characteristic length scales which will provide useful insight into possible magnetization processes depending on the magnet's size.

Let us assume that M_s is constant over the magnetic body (conditions 2 and 3 in Sect. 2). We introduce the external and demagnetizing field in dimensionless form $\mathbf{h}_{\text{ext}} = \mathbf{H}_{\text{ext}}/M_s$ and $\mathbf{h}_{\text{demag}} = \mathbf{H}_{\text{demag}}/M_s$ and rescale the length $\tilde{x} = x/L$, where L is the sample extension. Let us choose L so that $L^3 = V$. We also normalize the Gibbs free energy $\tilde{E}_{\text{tot}} = E_{\text{tot}}/(\mu_0 M_s^2 V)$. The normalization factor, $\mu_0 M_s^2 V$, is proportional to the magnetostatic self energy of fully magnetized sample. The energy contributions in dimensionless form are

$$\tilde{E}_{\text{ex}} = \int_{\tilde{V}} \frac{l_{\text{ex}}^2}{L^2} \left[(\tilde{\nabla} m_x)^2 + (\tilde{\nabla} m_y)^2 + (\tilde{\nabla} m_z)^2 \right] d\tilde{V}, \quad (92)$$

$$\tilde{E}_{\text{ext}} = - \int_{\tilde{V}} \mathbf{m} \cdot \mathbf{h}_{\text{ext}} d\tilde{V}, \quad (93)$$

$$\tilde{E}_{\text{demag}} = - \frac{1}{2} \int_{\tilde{V}} \mathbf{m} \cdot \mathbf{h}_{\text{demag}} d\tilde{V}, \quad (94)$$

$$\tilde{E}_{\text{ani}} = - \int_{\tilde{V}} \frac{K_1}{\mu_0 M_s^2} (\mathbf{c} \cdot \mathbf{m})^2 d\tilde{V}, \quad (95)$$

where \tilde{V} is the domain after transformation of the length. Further, we assumed uniaxial magnetic anisotropy, and neglected magnetoelastic coupling and magnetostriction. The constant l_{ex} in (92) is defined in the following section.

4.1 Exchange length

In (92) we introduced the exchange length

$$l_{\text{ex}} = \sqrt{\frac{A}{\mu_0 M_s^2}}. \quad (96)$$

It describe the relative importance of the exchange energy with respect to the magnetostatic energy. Inspecting the factor $(l_{\text{ex}}/L)^2$ in front of the brackets in (92), we see that the exchange energy contribution increases with decreasing sample size L . The smaller the sample the higher is the expense of exchange energy for non uniform magnetization. Therefore small samples show a uniform magnetization. If the magnetization remains parallel during switching the Stoner-Wohlfarth [58] model can be applied. In the literature the exchange length is either defined by (96) [59] or by $l'_{\text{ex}} = \sqrt{2A/(\mu_0 M_s^2)}$ [60].

4.2 Critical diameter for uniform rotation

In a sphere the magnetization reverses uniformly if its diameter is below $D \leq D_{\text{crit}} = 10.2l_{\text{ex}}$ [59]. During uniform rotation of the magnetization the exchange energy is zero and the magnetostatic energy remains constant. It is possible to lower the magnetostatic energy during reversal by magnetization curling. Then the magnetization becomes nonuniform at the expense of exchange energy. The total energy will be smaller than for uniform rotation if the sphere diameter, D , is larger than D_{crit} . Nonuniform reversal decreases

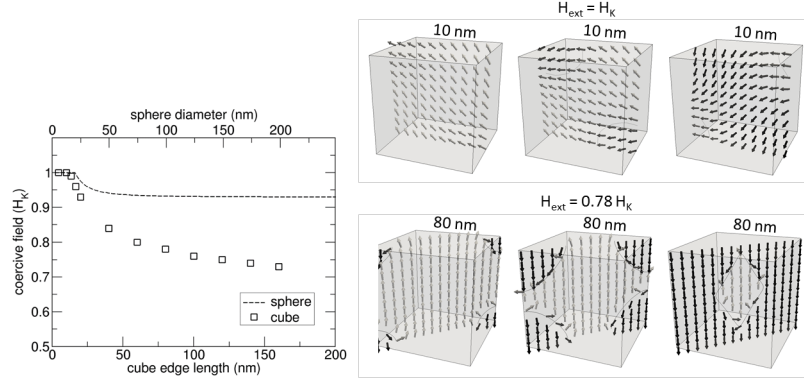


Fig. 6 Computed grain size dependence of the coercive field of a perfect $\text{Nd}_2\text{Fe}_{14}\text{B}$ cube at room temperature ($K_1 = 4.9 \text{ MJ/m}^3$, $\mu_0 M_s = 1.61 \text{ T}$, $A = 8 \text{ pJ/m}$, the mesh size is $h = 0.86\sqrt{A/K_1} = 1.1 \text{ nm}$, the external field is applied at an angle of 10^{-4} rad with respect to the easy axis). The sample dimensions are $L \times L \times L \text{ nm}^3$. Left: Switching field as function of L in units of H_K . The squares give the switching field of the cube. The dashed line is the theoretical switching field of a sphere with the same volume. A switching field smaller than H_K indicates nonuniform reversal. Right: Snap shots of the magnetic states during switching for $L = 10 \text{ nm}$ and $L = 80 \text{ nm}$.

the switching field as compared to uniform rotation. The switching fields of a sphere are [59]

$$H_c = \frac{2K_1}{\mu_0 M_s} \text{ for } D \leq D_{\text{crit}}. \quad (97)$$

$$H_c = \frac{2K_1}{\mu_0 M_s} - \frac{1}{3}M_s + \frac{34.66A}{\mu_0 M_s D^2} \text{ for } D > D_{\text{crit}}. \quad (98)$$

In cuboids and particles with polyhedral shape the nonuniform demagnetizing field causes a twist of the magnetization near edges or corners [61]. As a consequence nonuniform reversal occurs for particle sizes smaller than D_{crit} . The interplay between exchange energy and magnetostatic energy also causes a size dependence of the switching field [62, 63].

Grain size dependence of the coercive field. The coercive field of permanent magnets decreases with increasing grain size. This can be explained by the different scaling of the energy terms [63, 64]. The smaller the magnet the more dominant is the exchange term. Thus it costs more energy to form a domain wall. To achieve magnetization reversal the Zeeman energy of the reversed magnetization in the nucleus needs to be higher. This can be accomplished by a larger external field. Fig. 6 shows the switching field a $\text{Nd}_2\text{Fe}_{14}\text{B}$ cube as a function of its edge length. In addition we give the theoretical switching field for a sphere with the same volume according to (97) and (98). Magnetization reversal occurs by nucleation and expansion of reversed domains unless the hard magnetic cube is smaller than $6l_{\text{ex}}$.

4.3 Wall parameter

The square root of the ratio of the exchange length and the prefactor of the crystal anisotropy energy gives another critical length. The Bloch wall parameter

$$\delta_0 = \sqrt{\frac{A}{K}} \quad (99)$$

denotes the relative importance of the exchange energy versus crystalline anisotropy energy. It determines the width of the transition of the magnetization between two magnetic domains. In a Bloch wall the magnetization rotates in a way so that no magnetic volume charges are created. The mutual competition between exchange and anisotropy determines the domain wall width: Minimizing the exchange energy which favors wide transition regions whereas minimizing the crystal anisotropy energy favors narrow transition regions. In a bulk uniaxial material the wall width is $\delta_B = \pi\delta_0$.

4.3.1 Single domain size

With increasing particle the prefactor $(l_{\text{ex}}/L)^2$ for the exchange energy in (92) becomes smaller. A large particle can break up into magnetic domains because the expense of exchange energy is smaller than the gain in magnetostatic energy. In addition to the exchange energy the transition of the magnetization in the domain wall also increases the crystal anisotropy energy. The wall energy per unit area is $4\sqrt{AK_1}$. The energy of uniformly magnetized cube is its magnetostatic energy, $E_{\text{demag1}} = \mu_0 M_s^2 L^3 / 6$. In the two domain state the magnetostatic energy is roughly one half of this value, $E_{\text{demag2}} = \mu_0 M_s^2 L^3 / 12$. The energy of the wall is $E_{\text{wall2}} = 4\sqrt{AK_1} L^2$. Equating the energy of the single domain state, E_{demag1} , with the energy of the two domain state, $E_{\text{demag2}} + E_{\text{wall2}}$, and solving for L gives the single domain size of a cube

$$L_{\text{SD}} \approx \frac{48\sqrt{AK_1}}{\mu_0 M_s^2}. \quad (100)$$

The above equation simply means that the energy of a ferromagnetic cube with an a size $L > L_{\text{SD}}$ is lower in a the two domain state than in the uniformly magnetized state. A thermally demagnetized sample with $L > L_{\text{SD}}$ most likely will be in a multidomain state.

We have to keep in mind that the magnetic state of a magnet depends on its history and whether local or global minima can be accessed over the energy barriers that separate the different minima. The following situations may arise:

(1) A particle in its thermally demagnetized state is multidomain although $L < L_{\text{SD}}$ [65]. When cooling from the Curie temperature a particle with $L < L_{\text{SD}}$ may end up in a multidomain state. Although the single domain

state has a lower energy it cannot be accessed because it is separated from the multidomain state by a high energy barrier. This behavior is observed in small $\text{Nd}_2\text{Fe}_{14}\text{B}$ particles [65].

(2) An initially saturated cube with $L > L_{\text{SD}}$ will not break up into domains spontaneously if its anisotropy field is larger than the demagnetizing field. The sample will remain in an almost uniform state until a reversed domain is nucleated.

(3) Magnetization reversal of a cube with $L < L_{\text{SD}}$ will be non-uniform. Switching occurs by the nucleation and expansion of a reversed domain for a particle size down to about $5l_{\text{ex}}$. For example in $\text{Nd}_2\text{Fe}_{14}\text{B}$ the single domain limit is $L_{\text{SD}} \approx 146$ nm, the exchange length is $l_{\text{ex}} = 1.97$ nm. The simulation presented in Fig. 6 shows the transition from uniform to nonuniform reversal which occurs at $L \approx 6l_{\text{ex}}$.

4.4 Mesh size in micromagnetic simulations

The required minimum mesh size in micromagnetic simulations depends on the process that should be described by the simulations. Here a few examples:

(1) For computing the switching field of a magnetic particle we need to describe the formation of a reversed nucleus. A reversed nucleus is formed near edges or corners where the demagnetizing field is high. We have to resolve the rotations of the magnetization that eventually form the reversed nucleus. The required minimum mesh size has to be smaller than the exchange length [60].

(2) For the simulation of domain wall motion the transition of the magnetization between the domains needs to be resolved. A failure to do so will lead to an artificial pinning of the domain wall on the computational grid [66]. In hard magnetic materials the required minimum mesh size has to be smaller than the Bloch wall parameter.

(3) In soft magnetic elements with vanishing crystal or stress induced anisotropy the magnetization varies continuously [67]. The smooth transitions of the magnetization transitions can be resolved with a grid size larger than the exchange length. Care has to be taken if vortices play a role in the magnetization process to be studied. Then artificial pinning of vortex cores on the computational grid [66] has to be avoided.

5 Brown's micromagnetic equation

In the following we will derive the equilibrium equations for the magnetization. The total Gibbs free energy of a magnet is a functional of $\mathbf{m}(\mathbf{x})$. To compute an equilibrium state we have to find the function $\mathbf{m}(\mathbf{x})$ that

minimizes E_{tot} taking into account $|\mathbf{m}(\mathbf{x})| = 1$. In addition the boundary conditions

$$\nabla m_x \cdot \mathbf{n} = 0, \quad \nabla m_y \cdot \mathbf{n} = 0, \quad \text{and} \quad \nabla m_z \cdot \mathbf{n} = 0 \quad (101)$$

hold, where \mathbf{n} is the surface normal. The boundary conditions follow from (11) and the respective equations for y and z and applying Green's first identity to each term of (14). The boundary conditions (101) can also be understood intuitively [15]. To be in equilibrium a magnetic moment at the surface has to be parallel with its neighbor inside when there is no surface anisotropy. Otherwise there is an exchange torque on the surface spin.

Most problems in micromagnetics can only be solved numerically. Instead of solving the Euler-Lagrange equation that results from the variation of (91) numerically we directly solve the variational problem. Direct methods [68, 69] represent the unknown function by a set of discrete variables. The minimization of the energy with respect to these variables gives an approximate solution to the variational problem. Two well-known techniques are the Euler method and the Ritz method. Both are used in numerical micromagnetics.

5.1 Euler method: Finite differences

In finite difference micromagnetics the solution $\mathbf{m}(\mathbf{x})$ is sampled on points (x_i, y_j, z_k) so that $\mathbf{m}_{ijk} = \mathbf{m}(x_i, y_j, z_k)$. On a regular grid with spacing h the positions of the grid points are $x_i = x_0 + ih$, $y_j = x_0 + jh$, and $z_k = x_0 + kh$. The points (x_i, y_j, z_k) are the cell centers of the computational grid. The magnetization is assumed to be constant within each cell. To obtain an approximation of the energy functional we replace the integral by a sum over all grid points, $\mathbf{m}(\mathbf{x})$ by \mathbf{m}_{ijk} , and the spatial derivatives of $\mathbf{m}(\mathbf{x})$ with the finite difference quotients. The approximated solution values \mathbf{m}_{ijk} are the unknowns of an algebraic minimization problem. The indices i , j , and k run from 1 to the number of grid points N_x , N_y , N_z in x , y , and z direction, respectively. In the following we will derive the equilibrium equations whereby for simplicity we will not take into account the magnetoelastic coupling energy and the magnetostrictive self energy.

We can approximate the exchange energy (14) on the finite difference grid as [70]

$$E_{\text{ex}} \approx h^3 \sum_{ijk} A_{ijk} \left[\left(\frac{m_{x,i+1jk} - m_{x,ijk}}{h} \right)^2 + \dots \right], \quad (102)$$

where we introduced the notation $A_{ijk} = A(x_i, y_j, z_k)$. The bracket on the right hand side of (102) contains 9 terms. We explicitly give only the first term. The other 8 terms are of similar form. Similarly, we can approximate the Zeeman energy (32)

$$E_{\text{ext}} \approx -\mu_0 h^3 \sum_{ijk} M_{s,ijk} (\mathbf{m}_{ijk} \cdot \mathbf{H}_{\text{ext},ijk}). \quad (103)$$

To approximate the magnetostatic energy we use (42) and (45). Replacing the integrals with sums over the computational cell we obtain

$$E_{\text{demag}} \approx \frac{\mu_0}{8\pi} \sum_{ijk} \sum_{i'j'k'} M_{s,ijk} M_{s,i'j'k'} \oint_{\partial V_{ijk}} \oint_{\partial V_{i'j'k'}} \frac{(\mathbf{m}_{ijk} \cdot \mathbf{n})(\mathbf{m}_{i'j'k'} \cdot \mathbf{n}')}{|\mathbf{x} - \mathbf{x}'|} dS dS'. \quad (104)$$

The volume integrals in (42) and (45) vanish when we assume that $\mathbf{m}(\mathbf{x})$ is constant within each computational cell ijk . The magnetostatic energy is often expressed in terms of the demagnetizing tensor $\mathbf{N}_{ijk,i'j'k'}$

$$E_{\text{demag}} \approx \frac{\mu_0}{2} h^3 \sum_{ijk} \sum_{i'j'k'} M_{s,ijk} \mathbf{m}_{ijk}^T \mathbf{N}_{ijk,i'j'k'} \mathbf{m}_{i'j'k'} M_{s,i'j'k'} \quad (105)$$

We approximate the anisotropy energy (60) by

$$E_{\text{ani}} \approx h^3 \sum_{ijk} e_{\text{ani}}(\mathbf{m}_{ijk}). \quad (106)$$

The total energy is now a function of the unknowns \mathbf{m}_{ijk} . The constraint (5) is approximated by

$$|\mathbf{m}_{ijk}| = 1 \quad (107)$$

where ijk runs over all computational cells. We obtain the equilibrium equations from differentiation

$$\frac{\partial}{\partial \mathbf{m}_{ijk}} \left[E_{\text{tot}}(\dots, \mathbf{m}_{ijk}, \dots) + \sum_{ijk} \frac{L_{ijk}}{2} (\mathbf{m}_{ijk} \cdot \mathbf{m}_{ijk} - 1) \right] = 0. \quad (108)$$

In the brackets we added a Lagrange function to take care of the constraints (107). L_{ijk} are Lagrange multipliers. From (108) we obtain the following set of equations for the unknowns \mathbf{m}_{ijk}

$$\begin{aligned} & -2A_{ijk} h^3 \left[\frac{\mathbf{m}_{i-1jk} - 2\mathbf{m}_{ijk} + \mathbf{m}_{i+1jk}}{h^2} + \dots \right] \\ & - \mu_0 M_{s,ijk} h^3 \mathbf{H}_{\text{ext},ijk} \\ & + \mu_0 M_{s,ijk} h^3 \sum_{i'j'k'} \mathbf{N}_{ijk,i'j'k'} \mathbf{m}_{i'j'k'} M_{s,i'j'k'} \\ & + h^3 \frac{\partial e_{\text{ani}}}{\partial \mathbf{m}_{ijk}} = -L_{ijk} \mathbf{m}_{ijk}. \end{aligned} \quad (109)$$

The term in brackets is the Laplacian discretized on a regular grid. First order equilibrium conditions require also zero derivative with respect to the

Lagrange multipliers. This gives back the constraints (107). It is convenient to collect all terms with the dimensions of A/m to the effective field

$$\mathbf{H}_{\text{eff},ijk} = \mathbf{H}_{\text{ex},ijk} + \mathbf{H}_{\text{ext},ijk} + \mathbf{H}_{\text{demag},ijk} + \mathbf{H}_{\text{ani},ijk}. \quad (110)$$

The exchange field, the magnetostatic field, and the anisotropy field at the computational cell ijk are

$$\mathbf{H}_{\text{ex},ijk} = \frac{2A_{ijk}}{\mu_0 M_{s,ijk}} \left[\frac{\mathbf{m}_{i-1jk} - 2\mathbf{m}_{ijk} + \mathbf{m}_{i+1jk}}{h^2} + \dots \right] \quad (111)$$

$$\mathbf{H}_{\text{demag},ijk} = - \sum_{i'j'k'} \mathbf{N}_{ijk,i'j'k'} \mathbf{m}_{i'j'k'} M_{s,i'j'k'} \quad (112)$$

$$\mathbf{H}_{\text{ani},ijk} = - \frac{1}{\mu_0 M_{s,ijk}} \frac{\partial e_{\text{ani}}}{\partial \mathbf{m}_{ijk}}, \quad (113)$$

respectively. The evaluation of the exchange field (111) requires values of \mathbf{m}_{ijk} outside the index range $[1, N_x] \times [1, N_y] \times [1, N_z]$. These values are obtained by mirroring the values of the surface cell at the boundary. This method of evaluating the exchange field takes into account the boundary conditions (101).

Using the effective field we can rewrite the equilibrium equations

$$\mu_0 M_{s,ijk} h^3 \mathbf{H}_{\text{eff},ijk} = L_{ijk} \mathbf{m}_{ijk}. \quad (114)$$

Equation (114) states that the effective field is parallel to the magnetization at each computational cell. Instead of (114) we can also write

$$\mu_0 M_{s,ijk} h^3 \mathbf{m}_{ijk} \times \mathbf{H}_{\text{eff},ijk} = 0. \quad (115)$$

The expression $M_{s,ijk} h^3 \mathbf{m}_{ijk}$ is the magnetic moment of computational cell ijk . Comparison with (1) shows that in equilibrium the torque for each small volume element h^3 (or computational cell) has to be zero. The constraints (107) also have to be fulfilled in equilibrium.

5.2 Ritz method: Finite elements

Within the framework of the Ritz method the solution is assumed to depend on a few adjustable parameters. The minimization of the total Gibbs free energy with respect to these parameters gives an approximate solution [15, 16].

Most finite element solvers for micromagnetics use a magnetic scalar potential for the computation of the magnetostatic energy. This goes back to Brown [16] who introduced an expression for the magnetostatic energy, $E'_{\text{demag}}(\mathbf{m}, U')$, in terms of the scalar potential for the computation of equi-

librium magnetic states using the Ritz method. We replace $E_{\text{demag}}(\mathbf{m})$ with $E'_{\text{demag}}(\mathbf{m}, U')$, as introduced in (55), in the expression for the total energy. The vector $\mathbf{m}(\mathbf{x})$ is expanded by means of basis functions φ_i with local support around node \mathbf{x}_i

$$\mathbf{m}^{\text{fe}}(\mathbf{x}) = \sum_i \varphi_i(\mathbf{x}) \mathbf{m}_i. \quad (116)$$

Similarly, we expand the magnetic scalar potential

$$U^{\text{fe}}(\mathbf{x}) = U'(\mathbf{x}) = \sum_i \varphi_i(\mathbf{x}) U_i. \quad (117)$$

The index i runs over all nodes of the finite element mesh. The expansion coefficients \mathbf{m}_i and U_i are the nodal values of the unit magnetization vector and the magnetic scalar potential respectively. We assume that the constraint $|\mathbf{m}| = 1$ is fulfilled only at the nodes of the finite element mesh. We introduce a Lagrange function; L_i are the Lagrange multipliers at the nodes of the finite element mesh. By differentiation with respect to \mathbf{m}_i , U_i , and L_i , we obtain the equilibrium conditions

$$\frac{\partial}{\partial \mathbf{m}_i} \left[E_{\text{tot}}(\dots, \mathbf{m}_i, U_i \dots) + \sum_i \frac{L_i}{2} (\mathbf{m}_i \cdot \mathbf{m}_i - 1) \right] = 0, \quad (118)$$

$$\frac{\partial}{\partial U_i} \left[E_{\text{tot}}(\dots, \mathbf{m}_i, U_i \dots) + \sum_i \frac{L_i}{2} (\mathbf{m}_i \cdot \mathbf{m}_i - 1) \right] = 0, \quad (119)$$

$$\frac{\partial}{\partial L_i} \left[E_{\text{tot}}(\dots, \mathbf{m}_i, U_i \dots) + \sum_i \frac{L_i}{2} (\mathbf{m}_i \cdot \mathbf{m}_i - 1) \right] = 0. \quad (120)$$

From (118) we obtain the following set of equations for the unknowns \mathbf{m}_i

$$\begin{aligned} & 2 \sum_j \int_V A \nabla \varphi_i \nabla \varphi_j dV \mathbf{m}_j \\ & - \int_V \mu_0 M_s \mathbf{H}_{\text{ext}} \varphi_i dV \\ & + \int_V \mu_0 M_s \nabla U \varphi_i dV \\ & + \int_V \frac{\partial e_{\text{ani}}(\sum_j \varphi_j \mathbf{m}_j)}{\partial \mathbf{m}_i} dV = -L_i \mathbf{m}_i. \end{aligned} \quad (121)$$

Equation (119) is the discretized form of the partial differential equation (50) for the magnetic scalar potential. Equation (120) gives back the constraint $|\mathbf{m}| = 1$.

In the following we assume that \mathbf{H}_{ext} and $\mathbf{H}_{\text{demag}} = -\nabla U$ are constant over the support of basis function φ_i . Then we can introduce the effective field at the nodes of the finite element mesh

$$\begin{aligned} \mathbf{H}_{\text{eff},i} = & -\frac{2}{\mu_0 \mathcal{M}} \sum_j \int_V A \nabla \varphi_i \nabla \varphi_j dV \mathbf{m}_j \\ & + \mathbf{H}_{\text{ext}} + \mathbf{H}_{\text{demag}} - \frac{1}{\mu_0 \mathcal{M}} \int_V \frac{\partial e_{\text{ani}}}{\partial \mathbf{m}_i} dV, \end{aligned} \quad (122)$$

where $\mathcal{M} = \int_V M_s \varphi_i dV$. The equilibrium equations are

$$\mu_0 \mathcal{M} \mathbf{H}_{\text{eff},i} = L_i \mathbf{m}_i. \quad (123)$$

We can write the equilibrium conditions in terms of a cross product of the magnetic moment, $\mathcal{M} \mathbf{m}_i$, and the effective field at node i

$$\mu_0 \mathcal{M} \mathbf{m}_i \times \mathbf{H}_{\text{eff},i} = 0. \quad (124)$$

The system is in equilibrium if the torque equals zero and the constraint $|\mathbf{m}_i| = 1$ is fulfilled on all nodes of the finite element mesh.

Instead of a Lagrange function for keeping the constraint $|\mathbf{m}| = 1$ project methods [71] are commonly used in fast micromagnetic solvers [72]. In the iterative scheme for solving (124) the search direction \mathbf{d}_i^{k+1} is projected onto a plane perpendicular to \mathbf{m}_i^k . After each iteration k the vector \mathbf{m}_i^{k+1} is normalized.

6 Magnetization dynamics

Brown's equations describes the conditions for equilibrium. In many applications the response of the system to a time varying external field is important. The equations by Landau-Lifshitz [73] or Gilbert [74] describes the time evolution of the magnetization. The Gilbert equation in Landau-Lifshitz form

$$\frac{\partial \mathbf{m}}{\partial t} = -\frac{|\gamma| \mu_0}{1 + \alpha^2} \mathbf{m} \times \mathbf{H}_{\text{eff}} - \frac{|\gamma| \mu_0 \alpha}{1 + \alpha^2} \mathbf{m} \times (\mathbf{m} \times \mathbf{H}_{\text{eff}}) \quad (125)$$

is widely used in numerical micromagnetics. Here $|\gamma| = 1.76086 \times 10^{11} \text{s}^{-1} \text{T}^{-1}$ is the gyromagnetic ratio and α is the Gilbert damping constant. In (125) the unit vector of the magnetization and the effective field at the grid point of a finite difference grid or finite element mesh may be used for \mathbf{m} and \mathbf{H}_{eff} . The first term of (125) describes the precession of the magnetization around the effective field. The last term of (125) describes the damping. The double cross product gives the motion of the magnetization towards the effective field.

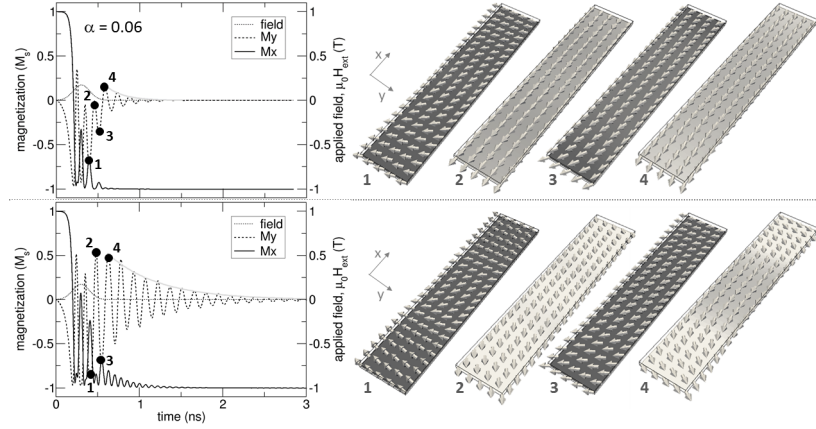


Fig. 7 Switching of a thin film nano-element by a short field pulse in the $(-1,-1,-1)$ direction for $\alpha = 0.06$ (top row) and $\alpha = 0.02$ (bottom row). ($K_1 = 0$, $\mu_0 M_s = 1$ T, $A = 10$ pJ/m, mesh size $h = 0.56\sqrt{A/(\mu_0 M_s^2)} = 2$ nm). The sample dimensions are $100 \times 20 \times 2$ nm³. The sample is originally magnetized in the $+x$ direction. Left: Magnetization as function of time. The thin dotted line gives the field pulse, $H_{\text{ext}}(t)$. Once the field is switched off damped oscillations occur which are clearly seen in $M_y(t)$. The bold grey line is a fit to the envelope of the magnetization component parallel to the short axis. Right: Transient magnetic states. The numbers correspond to the black dots in the plot of $M_y(t)$ on the left.

The interplay between the precession and the damping term leads to damped oscillations of the magnetization around its equilibrium state. In the limiting case of small deviations from equilibrium and uniform magnetization the amplitude of the oscillations decay as [75]

$$a(t) = C e^{-t/t_0}. \quad (126)$$

For small damping the oscillations decay time is [75]

$$t_0 = \frac{2}{\alpha \gamma \mu_0 M_s}. \quad (127)$$

Switching of a magnetic nano-elements. Small thin film nano-elements are key building blocks of magnetic sensor and storage applications. By application of a short field pulse a thin film nano-element can be switched. After reversal the system relaxes to its equilibrium state by damped oscillations. Fig. 7 shows the switching dynamics of a NiFe film with a length of 100 nm, a width of 20 nm, and a thickness of 2 nm. In equilibrium the magnetization is parallel to the long axis of the particle (x axis). A Gaussian field pulse (dotted line in Fig. 7) is applied in the $(-1,-1,-1)$ direction. After the field is switched off the magnetization oscillates towards the long axis of the film.

From of fit to the envelope of the magnetization component, $M_y(t)$, parallel to the short axes we derived the characteristic decay times of the oscillation which are $t_0 \approx 0.613$ ns and $t_0 \approx 0.204$ ns for a damping constant of $\alpha = 0.02$ and $\alpha = 0.06$, respectively. According to (127) the difference between the two relaxations times is a factor of 3, given by the ratio of the damping constants.

Acknowledgements The authors the Austrian Science Fund (FWF) under gant No. F4112 SFB ViCoM for financial support.

Appendix

The intrinsic material properties listed in Table 1 are taken from [76]. The exchange lengths and the wall parameter are calculated as follows: $l_{\text{ex}} = \sqrt{A/(\mu_0 M_s^2)}$, $\delta_0 = \sqrt{A/|K_1|}$.

Table 1 Intrinsic magnetic properties and characteristic lengths of selected magnetic materials.

Material	T_C (K)	$\mu_0 M_s$ (T)	A (pJ/m)	K_1 (kJ/m ³)	l_{ex} (nm)	δ_0 (nm)
Fe	1044	2.15	22	48	2.4	21
Co	1360	1.82	31	410	3.4	8.7
Ni	628	0.61	8	-5	5.2	40
Ni _{0.8} Fe _{0.2}	843	1.04	10	-1	3.4	100
CoPt	840	1.01	10	4900	3.5	1.4
Nd ₂ Fe ₁₄ B	588	1.61	8	4900	2.0	1.3
SmCo ₅	1020	1.08	12	17200	3.6	0.8
Sm ₂ Co ₁₇	1190	1.25	16	4200	3.6	2.0
Fe ₃ O ₄	860	0.6	7	-13	4.9	23

The examples given in Figures 3 to 7 were computed using the micro-magnetic simulation environment FIDIMAG [43]. FIDIMAG solves finite difference micromagnetic problems using a Python interface. The reader is encouraged to run computer experiments for further exploration of micro-magnetism. In the following we illustrate the use of the Python interface for simulating the switching dynamics of a magnetic nano-element (see Fig. 7). The function *relax_system* computes the initial magnetic state. The function *apply_field* computes the response of the magnetization under the influence of a time varying external field.

```
import numpy as np
from fidimag.micro import Sim
from fidimag.common import CuboidMesh
from fidimag.micro import UniformExchange, Demag
from fidimag.micro import TimeZeeman

mu0 = 4 * np.pi * 1e-7
A = 1.0e-11
```

```

Ms = 1./mu0

def relax_system(mesh):
    sim = Sim(mesh, name='relax')
    sim.set_tols(rtol=1e-10, atol=1e-10)
    sim.alpha = 0.5
    sim.gamma = 2.211e5
    sim.Ms = Ms
    sim.do_precession = False
    sim.set_m((0.577350269, 0.577350269, 0.577350269))

    sim.add(UniformExchange(A=A))
    sim.add(Demag())

    sim.relax()
    np.save('m0.npy', sim.spin)

def apply_field(mesh):
    sim = Sim(mesh, name='dyn')
    sim.set_tols(rtol=1e-10, atol=1e-10)
    sim.alpha = 0.02
    sim.gamma = 2.211e5
    sim.Ms = Ms
    sim.set_m(np.load('m0.npy'))

    sim.add(UniformExchange(A=A))
    sim.add(Demag())

    sigma = 0.1e-9
    def gaussian_fun(t):
        return np.exp(-0.5 * ((t-3*sigma) / sigma)**2)

    mT = 0.001 / mu0
    zeeman = TimeZeeman([-100 * mT, -100 * mT, -100 * mT], time_fun=
        gaussian_fun, name='H')
    sim.add(zeeman, save_field=True)
    sim.relax(dt=1.e-12, max_steps=10000)

if __name__ == '__main__':
    mesh = CuboidMesh(nx=50, ny=10, nz=1, dx=2, dy=2, dz=2, unit_length=1e
        -9)
    relax_system(mesh)
    apply_field(mesh)

```

References

1. H. Fukuda, Y. Nakatani, IEEE Transactions on Magnetism **48**(11), 3895 (2012)
2. S. Greaves, T. Katayama, Y. Kanai, H. Muraoka, IEEE Transactions on Magnetism **51**(4), 1 (2015)
3. H. Wang, T. Katayama, K.S. Chan, Y. Kanai, Z. Yuan, S. Shafidah, IEEE Transactions on Magnetism **51**(11), 1 (2015)
4. A. Kovacs, H. Oezelt, M.E. Schabes, T. Schrefl, Journal of Applied Physics **120**(1), 013902 (2016)
5. C. Vogler, C. Abert, F. Bruckner, D. Suess, D. Praetorius, Journal of Applied Physics **119**(22), 223903 (2016)
6. A. Makarov, V. Sverdlov, D. Osintsev, S. Selberherr, IEEE Transactions on Magnetism **48**(4), 1289 (2012)

7. B. Lacoste, M.M. de Castro, T. Devolder, R. Sousa, L. Buda-Prejbeanu, S. Auffret, U. Ebels, C. Ducruet, I. Prejbeanu, L. Vila, et al., *Physical Review B* **90**(22), 224404 (2014)
8. Z. Hou, A. Silva, D. Leitao, R. Ferreira, S. Cardoso, P. Freitas, *Physica B: Condensed Matter* **435**, 163 (2014)
9. D.C. Leitao, A.V. Silva, E. Paz, R. Ferreira, S. Cardoso, P.P. Freitas, *Nanotechnology* **27**(4), 045501 (2015)
10. I. Ennen, D. Kappe, T. Rempel, C. Glenske, A. Hütten, *Sensors* **16**(6), 904 (2016)
11. H. Sepehri-Amin, T. Ohkubo, S. Nagashima, M. Yano, T. Shoji, A. Kato, T. Schrefl, K. Hono, *Acta Materialia* **61**(17), 6622 (2013)
12. S. Bance, H. Oezelt, T. Schrefl, M. Winklhofer, G. Hrkac, G. Zimanyi, O. Gutfleisch, R. Evans, R. Chantrell, T. Shoji, et al., *Applied Physics Letters* **105**(19), 192401 (2014)
13. H. Fukunaga, R. Hori, M. Nakano, T. Yanai, R. Kato, Y. Nakazawa, *Journal of Applied Physics* **117**(17), 17A729 (2015)
14. R.F. Evans, W.J. Fan, P. Chureemart, T.A. Ostler, M.O. Ellis, R.W. Chantrell, *Journal of Physics: Condensed Matter* **26**(10), 103202 (2014)
15. W.F. Brown Jr, *Journal of Applied Physics* **30**(4), S62 (1959)
16. W.F. Brown, *Micromagnetics* (Interscience Publishers, New York, London, 1963)
17. W. Heisenberg, *Zeitschrift für Physik* **49**(9), 619 (1928). DOI 10.1007/BF01328601. URL <http://dx.doi.org/10.1007/BF01328601>
18. V. Vleck, *The theory of electric and magnetic susceptibilities* (Oxford University Press, 1932)
19. Y. Harashima, K. Terakura, H. Kino, S. Ishibashi, T. Miyake, *Phys. Rev. B* **92**, 184426 (2015). DOI 10.1103/PhysRevB.92.184426. URL <http://link.aps.org/doi/10.1103/PhysRevB.92.184426>
20. B.D. Cullity, C.D. Graham, *Introduction to magnetic materials*, second edition edn. (IEEE Press, 2009)
21. E. Kneller, *Ferromagnetismus* (Springer, Berlin, Göttingen, Heidelberg, 1962)
22. C. Kittel, *Introduction to Solid State Physics*, eighth edition edn. (John Wiley & Sons, 2005)
23. P. Talagala, P. Fodor, D. Haddad, R. Naik, L. Wenger, P. Vaishnav, V. Naik, *Physical Review B* **66**(14), 144426 (2002)
24. C. Eyrich, A. Zamani, W. Huttema, M. Arora, D. Harrison, F. Rashidi, D. Broun, B. Heinrich, O. Mryasov, M. Ahlberg, et al., *Physical Review B* **90**(23), 235408 (2014)
25. J. Weissmüller, R.D. McMichael, A. Michels, R. Shull, *Journal of research of the National Institute of Standards and Technology* **104**(3), 261 (1999)
26. K. Ono, N. Inami, K. Saito, Y. Takeichi, M. Yano, T. Shoji, A. Manabe, A. Kato, Y. Kaneko, D. Kawana, et al., *Journal of Applied Physics* **115**(17), 17A714 (2014)
27. N. Smith, D. Markham, D. LaTourette, *Journal of applied physics* **65**(11), 4362 (1989)
28. J. Livingston, M. McConnell, *Journal of Applied Physics* **43**(11), 4756 (1972)
29. J. Livingston, *Journal of applied physics* **57**(8), 4137 (1985)
30. S. Newnham, J. Jakubovics, A. Daykin, *Journal of magnetism and magnetic materials* **157**, 39 (1996)
31. J.D. Jackson, *Classical Electrodynamics*, third edition edn. (John Wiley & Sons, 1999)
32. C. Steele, *IEEE Transactions on Magnetics* **18**(2), 393 (1982)
33. K. Senanan, R. Victora, *Applied physics letters* **81**(20), 3822 (2002)
34. W.F. Brown Jr, *Journal of Applied Physics* **49**(3), 1937 (1978)
35. A. LaBonte, *Journal of Applied Physics* **40**(6), 2450 (1969)
36. M. Schabes, A. Aharoni, *IEEE Transactions on Magnetics* **23**(6), 3882 (1987)
37. A. Aharoni, *Journal of applied physics* **83**(6), 3432 (1998)

38. R. Dittrich, W. Scholz. Calculator for magnetostatic energy and demagnetizing factor. <http://www.magpar.net/static/magpar/doc/html/demagcalc.html> (2016). Accessed August 11, 2016
39. M. Sato, Y. Ishii, Journal of Applied Physics **66**(2), 983 (1989)
40. P. Asselin, A. Thiele, IEEE transactions on magnetics **22**(6), 1876 (1986)
41. M. Donahue, D. Porter, R. McMichael, J. Eicke, J. Appl. Phys **87**, 5520 (2000)
42. A. Vansteenkiste, J. Leliaert, M. Dvornik, M. Helsen, F. Garcia-Sanchez, B. Van Waeyenberge, Aip Advances **4**(10), 107133 (2014)
43. W. Wang, M.A. Bisotti, D. Cortes, T. Kluyver, M. Vousden, R. Pepper, O. Laslett, R. Carey, H. Fangohr. Fidimag 0.1: finite difference micro magnetic simulation environment, university of southampton. <http://computationalmodelling.github.io/fidimag/> (2016). Accessed July 1, 2016
44. C. Abert, G. Selke, B. Kruger, A. Drews, IEEE Transactions on Magnetism **48**(3), 1105 (2012)
45. S. Fu, W. Cui, M. Hu, R. Chang, M.J. Donahue, V. Lomakin, IEEE Transactions on Magnetism **52**(4), 1 (2016)
46. W. Scholz, J. Fidler, T. Schrefl, D. Suess, H. Forster, V. Tsiantos, et al., Computational Materials Science **28**(2), 366 (2003)
47. T. Fischbacher, M. Franchin, G. Bordignon, H. Fangohr, IEEE Transactions on Magnetism **43**(6), 2896 (2007)
48. C. Abert, L. Exl, F. Bruckner, A. Drews, D. Suess, Journal of Magnetism and Magnetic Materials **345**, 29 (2013)
49. R. Chang, S. Li, M. Lubarda, B. Livshitz, V. Lomakin, Journal of Applied Physics **109**(7), 07D358 (2011)
50. R. Cowburn, M. Welland, Physical Review B **58**(14), 9217 (1998)
51. D. Goll, G. Schütz, H. Kronmüller, Physical Review B **67**(9), 094414 (2003)
52. P. James, O. Eriksson, O. Hjortstam, B. Johansson, L. Nordström, Applied Physics Letters **76**(7), 915 (2000)
53. A. Hubert, R. Schäfer, *Magnetic Domains*, corrected, 3rd printing edn. (Springer, 2009)
54. O. Rand, V. Rovenskii, *Analytical Methods in Anisotropic Elasticity* (Birkhäuser, Boston, Basel, Berlin, 2005)
55. Y. Shu, M. Lin, K. Wu, Mechanics of Materials **36**(10), 975 (2004)
56. R.C. Peng, J.M. Hu, K. Momeni, J.J. Wang, L.Q. Chen, C.W. Nan, Scientific reports **6**, 27561 (2016)
57. Z. Zhao, M. Jamali, N. D'Souza, D. Zhang, S. Bandyopadhyay, J. Atulasimha, J.P. Wang, arXiv preprint arXiv:1602.05684 (2016)
58. E.C. Stoner, E. Wohlfarth, Philosophical Transactions of the Royal Society of London A: Mathematical, Physical and Engineering Sciences **240**(826), 599 (1948)
59. R. Skomski, Journal of Physics: Condensed Matter **15**(20), R841 (2003)
60. W. Rave, K. Ramstöck, A. Hubert, Journal of Magnetism and Magnetic Materials **183**(3), 329 (1998)
61. M.E. Schabes, H.N. Bertram, Journal of Applied Physics **64**(3), 1347 (1988)
62. H. Schmidts, H. Kronmüller, Journal of magnetism and magnetic materials **94**(1), 220 (1991)
63. S. Bance, B. Seebacher, T. Schrefl, L. Exl, M. Winklhofer, G. Hrkac, G. Zimanyi, T. Shoji, M. Yano, N. Sakuma, et al., Journal of Applied Physics **116**(23), 233903 (2014)
64. J. Thielsch, D. Suess, L. Schultz, O. Gutfleisch, Journal of Applied Physics **114**(22), 223909 (2013)
65. D. Crew, E. Girt, D. Suess, T. Schrefl, K. Krishnan, G. Thomas, M. Guilot, Physical Review B **66**(18), 184418 (2002)
66. M. Donahue, R. McMichael, Physica B: Condensed Matter **233**(4), 272 (1997)
67. R. Schäfer, Journal of magnetism and magnetic materials **215**, 652 (2000)

68. R. Courant, D. Hilbert, *Methods of mathematical physics* (Interscience Publishers, New York, 1953)
69. L. Komzsik, *Applied calculus of variations for engineers* (CRC Press, Boca Raton, London, New York, 2009)
70. R. Victora, *Journal of applied physics* **62**(10), 4220 (1987)
71. R. Cohen, S.Y. Lin, M. Luskin, *Computer Physics Communications* **53**(1-3), 455 (1989)
72. L. Exl, S. Bance, F. Reichel, T. Schrefl, H.P. Stimming, N.J. Mauser, *Journal of Applied Physics* **115**(17), 17D118 (2014)
73. L.D. Landau, E. Lifshitz, *Phys. Z. Sowjetunion* **8**(153), 101 (1935)
74. T. Gilbert, *Phys. Rev.* **100**, 1243 (1955)
75. J. Miltat, G. Albuquerque, A. Thiaville, *An Introduction to Micromagnetics in the Dynamic Regime* (Springer, 2002), pp. 1–34
76. J.M.D. Coey, *Magnetism and Magnetic Materials*: (Cambridge University Press, Cambridge, 2001). DOI 10.1017/CBO9780511845000. URL <https://www.cambridge.org/core/books/magnetism-and-magnetic-materials/AD3557E2D4538CAA8488A8C1057313BC>